



HAL
open science

Experimental study and modelling of the kinetic of biomass char gasification in a fluidized bed reactor

Mathieu Morin, Sébastien Pécate, Mehrdji Hemati

► To cite this version:

Mathieu Morin, Sébastien Pécate, Mehrdji Hemati. Experimental study and modelling of the kinetic of biomass char gasification in a fluidized bed reactor. *Chemical Engineering Research and Design*, 2018, 131, pp.488-505. 10.1016/j.cherd.2017.09.030 . hal-01963448

HAL Id: hal-01963448

<https://hal.science/hal-01963448>

Submitted on 21 Dec 2018

HAL is a multi-disciplinary open access archive for the deposit and dissemination of scientific research documents, whether they are published or not. The documents may come from teaching and research institutions in France or abroad, or from public or private research centers.

L'archive ouverte pluridisciplinaire **HAL**, est destinée au dépôt et à la diffusion de documents scientifiques de niveau recherche, publiés ou non, émanant des établissements d'enseignement et de recherche français ou étrangers, des laboratoires publics ou privés.



Open Archive Toulouse Archive Ouverte

OATAO is an open access repository that collects the work of Toulouse researchers and makes it freely available over the web where possible

This is an author's version published in: <http://oatao.univ-toulouse.fr/21130>

Official URL: <https://doi.org/10.1016/j.cherd.2017.09.030>

To cite this version:

Morin, Mathieu  and Pécate, Sébastien  and Hemati, Mehdi  *Experimental study and modelling of the kinetic of biomass char gasification in a fluidized bed reactor.* (2018) *Chemical Engineering Research and Design*, 131. 488-505. ISSN 0263-8762

Any correspondence concerning this service should be sent to the repository administrator: tech-oatao@listes-diff.inp-toulouse.fr

Experimental study and modelling of the kinetic of biomass char gasification in a fluidized bed reactor

Mathieu Morin*, Sébastien Pécate, Mehrdji Hémati

Laboratoire de Génie Chimique, Université de Toulouse, CNRS, INPT, UPS, 4 allée Emile Monso, 31432 Toulouse, France

A B S T R A C T

This work presents experimental data on the kinetic of steam gasification of biomass char in a fluidized bed reactor at atmospheric pressure. The char was obtained from fast pyrolysis of cylindrical beech stick in an annex batch fluidized bed reactor at 650 °C. The experiments were performed for temperatures in the range of 700–850 °C and steam partial pressures between 0.1 and 0.7 bars. The results showed that the char steam gasification is done in two steps. First, a thermal degradation of char takes place just after its introduction in the fluidized bed. This step leads to a partial conversion of the reactive solid and a formation of volatile products. Then, the new carbonaceous residue reacts with steam to produce syngas. The effect of hydrogen partial pressure up to 0.25 bars on the kinetic of char gasification was also investigated. The results revealed that the presence of H₂ inhibits the reaction of steam gasification. Besides, interactions also occur between char and H₂ which lead to the formation of CH₄ in the product gas. Moreover, as the hydrogen partial pressure increases, the methane production also increases. Finally, a modelling kinetic study including the inhibiting effect of H₂ showed that experimental data can be well-represented by the Shrinking Core Model with an activation energy and a reaction order with respect to steam equal to 123 kJ/mol and 0.62, respectively.

1. Introduction

Biomass is a possible alternative to the direct use of fossil fuel in gasification process as it has the advantage of being neutral in regard to the emission of greenhouse gas carbon dioxide. Recently, an increasing interest has been showed for the production of methane via Methanation process and “Biomass to Fisher-Tropsch Liquids”. Biomass gasification is a thermochemical conversion occurring at high temperatures with many simultaneous reactions. It occurs in two stages: (i) a pyrolysis step above 350 °C in which the biomass undergoes a thermal conversion leading to the formation of volatile products either condensable (steam and tars) or non-condensable (H₂, CO, CO₂, CH₄ and C₂H_x) and a solid residue called char (Di Blasi, 2008); (ii) a gasification step in which the char reacts with steam and carbon dioxide at temperatures greater than 700 °C to produce syngas.

Biomass gasification is an endothermic process. To maintain a fixed temperature in the reactor, a contribution of energy is required. The gasification technologies can be divided into two types depending on the way the heat is supplied to the gasifier (Ruiz et al., 2013; Gómez-Barea and Leckner, 2010). First, in autothermal or direct gasification, the heat is provided by partial combustion of the fuel in the gasifier itself. This process includes the fixed bed gasifiers (co- and counter-current) and the “bubbling fluidized bed” gasifiers. In these types of reactor, the biomass undergoes drying, pyrolysis and partial combustion of volatile matters and char and finally the gasification of char. In allothermal or indirect gasification the heat is obtained from a source outside of the gasifier. One of the most promising technologies of indirect gasification is dual or twin fluidized bed (FICFB: Fast Internally Circulating Fluidized Bed) (Hofbauer et al., 2002). FICFB process consists of two reactors: a dense fluidized bed endothermic gasifier (operating around

Nomenclature	
A_{SCM}	Pre-exponential factor for the SCM ($\text{mol m}^{-2} \text{Pa}^{-n} \text{s}^{-1}$)
E_α	Activation energy (J mol^{-1})
$f(X)$	Structure function (-)
M_c	Molar weight of carbon (kg mol^{-1})
n	Reaction order with respect to steam (-)
$\dot{n}_{carbon}(t)$	Carbon molar flow rate (mol min^{-1})
$n_i(t)$	Cumulative amount of component i during the time t (mol)
$\dot{n}_t(t)$	Instantaneous total molar flow rate (mol min^{-1})
\dot{n}_{N_2}	Molar flow rate of nitrogen at the entrance of the reactor (mol min^{-1})
$\dot{n}_i(t)$	Instantaneous molar flow rate of component i (mol min^{-1})
$(n_{carbon})_{char}$	Amount of introduced carbon in the reactor (mol)
$P_{H_2O,s}$	Steam partial pressure at the particle surface (Pa)
P_{H_2}	Hydrogen partial pressure (Pa)
R	Universal gas constant ($\text{J mol}^{-1} \text{K}^{-1}$)
$R_{\alpha pp}$	Apparent reaction rate for $X_c = 0.4$
$R_{\alpha pp}(P_{H_2})$	Apparent reaction rate for various H_2 partial pressures
$R_{\alpha pp}(P_{H_2} = 0)$	Apparent reaction rate for various steam partial pressures and $P_{H_2} = 0$ bar
R_0	Initial particle radius
T_p	Particle temperature (K)
U_{mf}	Minimum fluidization velocity (m s^{-1})
X_c	Carbon conversion rate (-)
x_c	Mass fraction of carbon in the char particle (-)
$x_{N_2}(t)$	Measured molar fraction of nitrogen at the reactor outlet (-)
$x_i(t)$	Molar fraction of component i (-)
Greek letters	
ε_p	Solid porosity (-)
ρ_α	Apparent density (kg m^{-3})
$\rho_{t,c}$	True density (kg m^{-3})
γ_i	Number of carbons in the component i
τ_{CSTR}	Residence time of the continuous flow stirred-tank reactors (min)

750–850 °C) that produces the syngas and an entrained bed exothermic combustor (operating at 900–950 °C) that burns a part of the residual char to provide heat to the gasifier. A solid bed material (sand, olivine or catalyst particles) is circulated between the two reactors to transfer the heat to the gasification (Gómez-Barea and Leckner, 2010).

During biomass gasification in FICFB, the char reacts with steam and carbon dioxide in the gasifier and with oxygen in the combustor. Information regarding the kinetic of biomass char gasification with steam in a fluidized bed reactor is then essential to better understand phenomena occurring inside the gasifier and to design this process.

Char gasification with steam corresponds to a complex chemical transformation which occurs in several steps: (1) the external transfer of steam from the bulk to the external surface of the particle, (2) the diffusion of steam through the ash layer and within the pores of the solid, (3) the steam chemisorption on an active site (adsorption), (4) the intrinsic chemical reaction, (5) the products desorption from the surface, (6) the diffusion of the products through the particle and ash layer and finally (7) the external transfer back of the products from the external surface to the bulk (Laurendeau, 1978; Szekeley et al., 1976). These different steps are strongly affected by the physicochemical properties

of char, the gasification temperature, the steam partial pressure and the size of the solid particles.

The physicochemical properties of char depend on the parent fuel and the pyrolysis operating conditions (Di Blasi, 2009; Morin et al., 2016). In a previous study (Morin et al., 2016), it was highlighted that the physicochemical properties and the reactivity of char is strongly dependent on the pyrolysis temperature, the heating rate and the biomass nature. It was found that these parameters influence hydrogen, oxygen, carbon and ash contents in the char as well as the presence of amorphous and aromatic carbon. Besides, a raise of the heating rate during the biomass pyrolysis increases the char reactivity while an increase in the final temperature decreases the reactivity. The presence of inorganic matters (i.e. ashes) in the char matrix is known to catalyze the reaction of gasification (Mermoud et al., 2006; Marquez-Montesinos et al., 2002; Dupont et al., 2016). For instance, by comparing the reactivity in steam gasification in TGA of nineteen biomasses prepared under the same pyrolysis conditions, Dupont et al. (2016) emphasized the catalytic effect of potassium (K) as well as the inhibiting effect of silicon (Si) and phosphorous (P). Hence, they concluded that the gasification rate may be correlated to the ratio $K/(P + Si)$.

Szekely et al. (1976) divided the gasification of a porous solid into three main regimes according to the temperature, the steam partial pressure and the char particles size. Regime I is established for low temperatures and char particles sizes so that the mass transfer rates (i.e. steam diffusion inside the pores and external transfer around the particle) are much faster than the intrinsic chemical reaction rate. In this regime, both the gas concentration and the gas temperature on the char surface sites are equal to those in the bulk gas. When the temperature and the char particles size are increased (Regime II), the reactive gas cannot completely penetrate into the particle and leads to steam concentration gradients inside the char. This Regime II is the transition regime where both the diffusion of steam and the intrinsic chemical reaction play a significant role. Finally, in Regime III which occurs at high temperatures, the intrinsic reactivity of the solid is very high and the steam molecules react at the particle surface as soon as they have passed the boundary layer around the particle. The external mass transfer is then the limiting step.

Table 1 presents several literature works on the kinetic of biomass char gasification with steam. Overall, in the literature, the influence of the gasification temperature and the steam partial pressure was investigated in the range of 550–1150 °C and 500–100,000 Pa. It is well-established that the gasification rate increases by increasing these two parameters (Marquez-Montesinos et al., 2002; Nandi and Onischak, 1985; Bhat et al., 2001; Klose and Wölki, 2005; Paviet et al., 2007; Groeneveld and van Swaaij, 1980; Ahmed and Gupta, 2011; Nilsson et al., 2014, 2012; Le and Kolaczowski, 2015; Kramb et al., 2014; Zhai et al., 2015; Barrio et al., 2001; Kojima et al., 1993; Hawley et al., 1983; Hémati and Laguerie, 1988; Woodruff and Weimer, 2013). Table 1 also shows that a large variety of particles sizes was investigated between 45 μm to 2 mm. This parameter mainly influences the diffusion of steam inside the pores and yields to gradients of concentration within the particle. Hence, to determine the intrinsic char-steam gasification kinetic, the authors (Bhat et al., 2001; Klose and Wölki, 2005; Paviet et al., 2007; Ahmed and Gupta, 2011; Nilsson et al., 2014, 2012; Zhai et al., 2015; Hawley et al., 1983; Hémati and Laguerie, 1988) minimized the effects of heat and mass transfers so that the reaction of gasification takes place in Regime I and for isothermal conditions. In the case of TGA analyses, it consists in determining the particles size, the mass of char in the crucible and the volume flow rate of the reactive gas in the apparatus for a constant temperature and steam partial pressure until no influence on the gasification rate was observed (Klose and Wölki, 2005; Paviet et al., 2007; Hémati and Laguerie, 1988). Other researchers (Nilsson et al., 2014, 2012; Hawley et al., 1983) calculated the effectiveness factor (ratio between the actual reaction rate and the intrinsic reaction rate) which must be close to the unity in Regime I. By and large, bibliographic works (Di Blasi, 2009; Bhat et al., 2001) agreed that kinetic experiments of the char gasification with both steam and CO_2 takes place in Regime I in the absence of any mass transfer limitations for temperatures up to 900 °C.

Table 1 – Literature review on the kinetic of biomass char gasification with steam.

Ref.	Pyrolysis conditions	Gasification operating conditions				Kinetic expression
		Reactor	Temp (°C)	Diam. (mm)	H ₂ O (%)	
Marquez-Montesinos et al. (2002)	Quartz tube furnace 700 °C N ₂ 2 h Peel grapefruit	TGA (P _{atm})	725–800	1–1.6	1.7–47.4	$\frac{dX}{dt} = A \times \exp\left(-\frac{E_a}{RT}\right) P_{H_2O}^n (1-X)$ $E_a = 134,000 - 201,000$ $n = 0.53 - 0.73$
Nandi and Onischak (1985)	Tube furnace, 732–927 °C 11 °C/min 30 min Maple, pine	TGA (21.7 bar)	649–927	–	50 (5% H ₂)	M (N₂–H₂O): $\frac{dX}{dt} = 5.55 \times 10^5 \times \exp\left(-\frac{177,000}{RT}\right) (1-X)$ M (N₂–He–H₂O): $\frac{dX}{dt} = 2.96 \times 10^6 \times \exp\left(-\frac{195,000}{RT}\right) (1-X)$ P (N₂–H₂O): $\frac{dX}{dt} = 1.72 \times 10^5 \times \exp\left(-\frac{170,000}{RT}\right) (1-X)$ P (N₂–He–H₂O): $\frac{dX}{dt} = 2.89 \times 10^5 \times \exp\left(-\frac{178,000}{RT}\right) (1-X)$
Nandi and Onischak (1985)	TGA 704–871 °C N ₂ , H ₂ O (H ₂) Maple, pine	TGA (21.7 bar)	704–871	–	50 (5% H ₂)	M (N₂–H₂O): $\frac{dX}{dt} = 4.03 \times 10^5 \times \exp\left(-\frac{167,000}{RT}\right) (1-X)$ M (N₂–He–H₂O): $\frac{dX}{dt} = 3.65 \times 10^5 \times \exp\left(-\frac{167,000}{RT}\right) (1-X)$ P (N₂–H₂O): $\frac{dX}{dt} = 2.14 \times 10^5 \times \exp\left(-\frac{164,000}{RT}\right) (1-X)$ P (N₂–He–H₂O): $\frac{dX}{dt} = 1.77 \times 10^6 \times \exp\left(-\frac{176,000}{RT}\right) (1-X)$
Bhat et al. (2001)	Batch Pyrolysis 600–700 °C N ₂ (P _{atm}) Rice husk	Tubular reactor (P _{atm})	750–900	Grain	100	$\frac{dX}{dt} = \frac{2.9 \times 10^{10}}{T} \times \exp\left(-\frac{200,325}{RT}\right) P_{H_2O} (1-X)$
Klose and Wölki (2005)	Vertical tube furnace 900 °C 3 °C/min 30 min Beech, oil palm	TGA (P _{atm})	720–780	<0.125	70	$r = \frac{k}{1 + \frac{K}{\exp\left(-\frac{\Delta H}{RT}\right) P_{H_2O}}}$ B: k = 2.1 × 10⁷ exp $\left(-\frac{196,000}{RT}\right)$ K = 2 × 10⁷ Pa ΔH = –35,000 J mol^{–1} OP: k = 1.2 × 10¹¹ exp $\left(-\frac{299,000}{RT}\right)$ K = 2.5 × 10⁶ Pa ΔH = –37,000 J mol^{–1}
Paviet et al. (2007)	Muffle furnace, 1000 °C, 100 °C/min Paper, wood, plastic, vegetable	Tubular Kiln (P _{atm})	900–1000	0.1–2	30–70	P: $\frac{dX}{dt} = \frac{6.6 \times 10^4}{1-0.75} \times \exp\left(-\frac{174,000}{RT}\right) \frac{P_{H_2O}}{P_T} (1-X) \sqrt{1 - \ln(1-X)}$ W: $\frac{dX}{dt} = \frac{6 \times 10^5}{1-0.86} \times \exp\left(-\frac{204,000}{RT}\right) \frac{P_{H_2O}}{P_T} (1-X) \sqrt{1 - 5 \ln(1-X)}$ Pl: $\frac{dX}{dt} = \frac{1 \times 10^5}{1-0.75} \times \exp\left(-\frac{185,000}{RT}\right) \frac{P_{H_2O}}{P_T} (1-X) \sqrt{1 - 5 \ln(1-X)}$ V: $\frac{dX}{dt} = \frac{8.1 \times 10^4}{1-0.67} \times \exp\left(-\frac{178,000}{RT}\right) \frac{P_{H_2O}}{P_T} (1-X) \sqrt{1 - 5 \ln(1-X)}$
Groeneveld and van Swaaij (1980)	Wood, N ₂ , Patm, 980 °C	TGA (P _{atm})	800–1000	–	0.5–22	$\frac{dX}{dt} = \frac{10^7}{(RT)^{0.7}} \times \exp\left(-\frac{217,100}{RT}\right) (P_{H_2O} + P_{CO_2})^{0.7} (1-X)$
Ahmed and Gupta (2011)	Reaction chamber 900 °C He (P _{atm}) 1 h Woodchip	Reaction chamber (2 bar)	900	–	30–75	30% H₂O: $\frac{dX}{dt} = 0.052 \times (1-X) \sqrt{1 - 16.71 \ln(1-X)}$ 45% H₂O: $\frac{dX}{dt} = 0.056 \times (1-X) \sqrt{1 - 10.53 \ln(1-X)}$ 60% H₂O: $\frac{dX}{dt} = 0.080 \times (1-X) \sqrt{1 - 3.80 \ln(1-X)}$ 75% H₂O: $\frac{dX}{dt} = 0.071 \times (1-X) \sqrt{1 - 4.95 \ln(1-X)}$

Nilsson et al. (2014)	Fluidized bed 760–900 °C N ₂ (P _{atm}) Olive tree	Fluidized bed (P _{atm})	760–840	1.9	20–40 (10% H ₂)	$\frac{dX}{dt} = \frac{k_1 P_{H_2O}}{1 + k_2 P_{H_2O} + k_3 P_{H_2}} \times \frac{1}{(1-0.20)} \times (1-X)^n$ $k_1 = 1.2 \times \exp\left(-\frac{137,000}{RT}\right)$ $k_2 = 6.19 \times 10^{-6} \times \exp\left(\frac{22,900}{RT}\right)$ $k_3 = 2.93 \times 10^{-5} \times \exp\left(\frac{24,100}{RT}\right)$ $n = 0.8 - 1.5$
Le and Kolaczowski (2015)	Gasification Pilot plant RDF	Packed bed (P _{atm})	800–900	0.306	30–70	$\frac{dX}{dt} = A \times \exp\left(-\frac{E_a}{RT}\right) P_{H_2O}^n \times (1-X)^{2/3}$ $A = 1.14 \times 10^4 - 3.53 \times 10^4 \text{ s}^{-1} \text{ bar}^{-n}$ $E_a = 96,000 - 106,000$ $n = 0.89 - 2.9$
Kramb et al. (2014)	TGA 750–850 °C H ₂ O–H ₂ Pine sawdust	TGA (P _{atm})	750–850	–	89–100 (0–10% H ₂)	$\frac{dX}{dt} = \frac{k_{1f} P_{H_2O}}{1 + \frac{k_{1f}}{k_3} P_{H_2O} + \frac{k_{1b}}{k_3} P_{H_2}} \left[\alpha \exp(-\xi X^2) + (1-X) \sqrt{1 - \varphi \ln(1-X)} \right]$ $k_{1f} = 1.9 \times 10^7 \exp\left(-\frac{200,000}{RT}\right) \quad \varphi = 3.9$ $k_{1b} = 2.9 \times 10^{10} \exp\left(-\frac{240,000}{RT}\right) \quad \alpha = 3.8$ $k_3 = 2.4 \times 10^9 \exp\left(-\frac{250,000}{RT}\right) \quad \xi = 24$
Zhai et al. (2015)	Muffle furnace 800 °C 40 min Rice husk	Drop tube furnace (P _{atm})	700–950	1.2	100	$\frac{dX}{dt} = 0.388 \times \exp\left(-\frac{66,500}{RT}\right) \times (1-X)^{2/3}$ $\frac{dX}{dt} = 3.34 \times \exp\left(-\frac{74,800}{RT}\right) \times (1-X)$
Barrio et al. (2001)	Macro TGA 600 °C 24 °C/min	Pressurized TGA (P _{atm})	750–950	0.045–0.063	5–100 (10–30% H ₂)	$\text{Be (N}_2\text{-H}_2\text{O): } \frac{dX}{dt} = 3.7 \times 10^5 \exp\left(-\frac{237,000}{RT}\right) P_{H_2O}^{0.57} (1-X)$ $\text{Bi (N}_2\text{-H}_2\text{O): } \frac{dX}{dt} = 4.8 \times 10^4 \times \exp\left(-\frac{211,000}{RT}\right) P_{H_2O}^{0.51} (1-X)$ $\frac{dX}{dt} = \frac{k_{1f} P_{H_2O}}{1 + \frac{k_{1f}}{k_3} P_{H_2O} + \frac{k_{1b}}{k_3} P_{H_2}} \times (1-X)$

Table 1 (Continued)

Ref.	Pyrolysis conditions	Gasification operating conditions				Kinetic expression $\frac{dX}{dt}$ (s ⁻¹), A (s ⁻¹ or s ⁻¹ Pa ⁻ⁿ), E _a (J mol ⁻¹)
		Reactor	Temp (°C)	Diam. (mm)	H ₂ O (%)	
	30 min Beech, birch					$\text{Be (N}_2 - \text{H}_2\text{O} - \text{H}_2\text{)}: \quad k_{1f} = 2 \times 10^2 \exp\left(-\frac{199,000}{RT}\right)$ $k_{1b} = 18 \exp\left(-\frac{146,000}{RT}\right)$ $k_3 = 8.4 \times 10^7 \exp\left(-\frac{225,000}{RT}\right)$ $\text{Bi (N}_2 - \text{H}_2\text{O} - \text{H}_2\text{)}: \quad k_{1f} = 7.6 \times 10^2 \exp\left(-\frac{199,000}{RT}\right)$ $k_{1b} = 2.1 \times 10^9 \exp\left(-\frac{284,000}{RT}\right)$ $k_3 = 1.6 \times 10^{10} \exp\left(-\frac{273,000}{RT}\right)$
Kojima et al. (1993)	Fluidized bed 850–950 °C Sawdust	Fluidized bed (P _{atm})	850–950	1–2	0–58	$\frac{dX}{dt} = 1773 \times \exp\left(-\frac{179,000}{RT}\right) p_{\text{H}_2\text{O}}^{0.41} \times (1 - X)$
Hawley et al. (1983)	700 °C N ₂ 10 min Poplar wood	Electric furnace (P _{atm})	550–685	1–2	45–100	$\frac{dX}{dt} = 6.57 \times \exp\left(-\frac{156,000}{RT}\right) P_{\text{H}_2\text{O}} \times f(X)$
Hémati and Laguerie (1988)	TGA 750–1000 °C N ₂ (P _{atm}) Sawdust	TGA (P _{atm})	650–750	0.250–0.315	25–100	$\frac{dX}{dt} = 2.17 \times 10^3 \exp\left(-\frac{198,000}{RT}\right) p_{\text{H}_2\text{O}}^{0.75} \times (1 - X)$
Nilsson et al. (2012)	Fluidized bed 800–900 °C Dried sewage sludge	Fluidized bed (P _{atm})	800–900	1.2	10–30	$\frac{dX}{dt} = 8731 \exp\left(-\frac{171,000}{RT}\right) p_{\text{H}_2\text{O}}^{0.33} \times (1 - X) (11.5X + 3.6) \exp(-3X^{1/2})$
Woodruff and Weimer (2013)	1000 °C 20 °C/min 20 min Switch grass	Fixed bed (P _{atm})	1000–1150	10 Section	20–100 (0–40% H ₂)	$\frac{dX}{dt} = \frac{K_1 P_{\text{H}_2\text{O}}}{1 + K_2 P_{\text{H}_2\text{O}} + K_3 P_{\text{H}_2}} \times (1 - X) \sqrt{1 - \varphi \ln(1 - X)}$ $K_1 = 2.51 \times 10^{-2} \exp\left(-\frac{112,600}{RT}\right)$ $K_2 = 6.74 \times 10^{-7} \times \exp\left(\frac{37,300}{RT}\right)$ $K_3 = 3.04 \times 10^{-6} \times \exp\left(\frac{36,600}{RT}\right)$ $\varphi = 4.3$
Septien et al. (2015)	Macro TGA 850 °C 100 °C/s Beech chips	Macro TGA (P _{atm})	750–950	<0.250	15–50	$\frac{dX}{dt} = 7.349 \times 10^7 \exp\left(-\frac{275,000}{RT}\right) p_{\text{H}_2\text{O}}^{0.65} \times (34.228X^6 - 69.460X^5 + 49.267X^4 - 7.903X^3 - 2.653X^2 + 1.633X + 0.345)$

Table 1 highlights that a wide range of biomasses (wood, paper, plastic, vegetable, rice husk, switchgrass, RDF...) as well as pyrolysis conditions (temperatures ranging from 600 to 1000 °C and heating rates between 3 and 100 °C/min) were applied during the pyrolysis. The char gasification with steam was performed in a large variety of reactors (TGA, packed bed, fluidized bed, drop tube furnace...). The obtained kinetic expressions combined to mass transfers and hydrodynamic phenomena may be used to model the char gasification in industrial conditions. For instance, Bates et al. (2016) proposed a transient char conversion model in oxygen-free gasification conditions in a fluidized bed reactor. In this case, they assumed that the char is consumed by gasification, combustion and attrition.

The most widely used treatment to represent the char-steam reaction for both coal char and biomass char is based on a simple global reaction (Di Blasi, 2009; Roberts and Harris, 2006; Hüttinger and Merdes, 1992):



Followed by the Water–Gas–Shift (WGS) reaction in the gas-phase which is close to the equilibrium during char steam gasification:



A part of the carbon dioxide from the WGS reaction may also react with char to produce carbon monoxide according to the Boudouard reaction:



The amount of CH₄ produced at atmospheric pressure during char-steam gasification is low and is usually neglected (Di Blasi, 2009).

In reality, Reaction (I) consists of a series of oxygen adsorption and desorption processes. The simplest reaction scheme to represent Reaction (I) is that an oxygen atom of the steam molecule is adsorbed on an active site of the carbon surface to give a carbon-oxygen complex C(O) which then further desorbs to produce CO. These steps are known as oxygen exchange mechanism and are expressed by the two following reactions:



The reactivity of char with steam can be described by the rate of a solid-state reaction according to the following expression (Vyazovkin et al., 2011; Khawam and Flanagan, 2010):

$$\frac{dX}{dt} = k(T_p) \cdot h(P_{\text{H}_2\text{O},s}) \cdot f(X) \quad (1)$$

where X , $P_{\text{H}_2\text{O},s}$ and T_p are respectively the conversion rate, the steam partial pressure at the particle surface (Pa), and the particle temperature (K). $f(X)$ is the reaction model also known as the structure function. $h(P_{\text{H}_2\text{O},s})$ is the steam partial pressure function which represents the effect of steam partial pressure on the reaction rate. $k(T_p)$ is the temperature dependent rate constant.

In the literature (Di Blasi, 2009), the majority of kinetic analyses consider Reaction (I) as a simple global reaction. In this case, $k(T_p)$ is described by an Arrhenius law and $h(P_{\text{O}_2,s})$ is given in the form of a power law:

$$k(T_p) \cdot h(P_{\text{H}_2\text{O},s}) = A \cdot \exp\left(-\frac{E_a}{RT_p}\right) \cdot P_{\text{H}_2\text{O},s}^n \quad (2)$$

where A is the pre-exponential factor, E_a is the activation energy (J mol⁻¹), R is the gas constant (J mol⁻¹ K⁻¹) and n is the reaction order with respect to steam.

From Table 1, this global kinetic model leads to activation energies ranging from 66,500 to 237,000 J/mol and reaction orders with respect

to steam between 0.33 and 1. According to Di Blasi (2009), this dispersion in the kinetic parameters is caused by different biomasses and char properties, pyrolysis conditions, amounts and compositions of ash, gasification conditions and devices of the experiment. It is important to note that several authors (Nandi and Onischak, 1985; Zhai et al., 2015) incorporated the dependence of the reactivity on the steam partial pressure into the pre-exponential factor so that the results are only valid for the gaseous mixture used in the experiment (Di Blasi, 2009).

In the case of steam gasification of coal char, some researchers (Roberts and Harris, 2006) have used a Langmuir–Hinshelwood formulation to represent the kinetic data. The simplest Langmuir–Hinshelwood formulation takes into account Reactions (IV) and (V) and is given by:

$$k(T_p) \cdot h(P_{\text{H}_2\text{O},s}) = R_{\text{global}} = \frac{k_{\text{IV}} P_{\text{H}_2\text{O},s}}{1 + \frac{k_{\text{IV}}}{k_{\text{V}}} \cdot P_{\text{H}_2\text{O},s}} \quad (3)$$

where k_{IV} and k_{V} are the rate constants of Reactions (IV) and (V), respectively and follow an Arrhenius law.

The hydrogen inhibition effect during the char gasification was also taken into account by some authors in the kinetic modelling (Nilsson et al., 2014; Kramb et al., 2014; Barrio et al., 2001; Woodruff and Weimer, 2013; Hüttinger, 1988; Lussier et al., 1998). Indeed, the presence of hydrogen is known to decrease the char reactivity with steam. This phenomenon may be explained by either the equilibrium of Reaction (IV) or by hydrogen adsorption on the active sites. Hence, the kinetic expression can be expressed as follows:

$$k(T_p) \cdot h(P_{\text{O}_2,s}) = R_{\text{global}} = \frac{k_{\text{IV}} P_{\text{H}_2\text{O}}}{1 + \frac{k_{\text{IV}}}{k_{\text{V}}} \cdot P_{\text{H}_2\text{O}} + f(P_{\text{H}_2})} \quad (4)$$

where P_{H_2} is the hydrogen partial pressure and $f(P_{\text{H}_2})$ is a function which depends on the selected mechanism for hydrogen inhibition.

Literature studies (Kramb et al., 2014; Barrio et al., 2001; Hüttinger, 1988; Lussier et al., 1998) mainly assume the oxygen-exchange mechanism to represent hydrogen inhibition which considers Reaction (IV) as reversible. $f(P_{\text{H}_2})$ is then expressed as:

$$f(P_{\text{H}_2}) = \frac{k_{-IV}}{k_{\text{V}}} \cdot P_{\text{H}_2} \quad (5)$$

In some cases, several authors (Nilsson et al., 2014; Woodruff and Weimer, 2013) reduced Eq. (4) to the following expression without considering any hydrogen inhibition mechanisms:

$$k(T_p) \cdot h(P_{\text{O}_2,s}) = R_{\text{global}} = \frac{K_1 P_{\text{H}_2\text{O}}}{1 + K_2 \cdot P_{\text{H}_2\text{O}} + K_3 \cdot P_{\text{H}_2}} \quad (6)$$

The char gasification with CO₂ (i.e. Boudouard reaction) has similarity to the char steam reaction as it also includes an oxygen exchange mechanism (Irfan et al., 2011). The Boudouard reaction was extensively studied in the literature (Di Blasi, 2009; Ahmed and Gupta, 2011; Nilsson et al., 2014, 2012; Irfan et al., 2011). The authors found that the char-CO₂ reaction is 3–4 times slower than the reaction with H₂O. Besides, in the case of coal char, several researchers (Groeneveld and van Swaaij, 1980; Roberts and Harris, 2007; Chen et al., 2015) studied the char gasification with mixtures of CO₂ and H₂O. For instance, Chen et al. (2015) found that the char gasification rate in a mixture of CO₂ and H₂O is lower than the sum of the reaction rates taken individually. Moreover, CO₂ and H₂O molecules may compete for the same active sites on the char surface. Roberts and Harris (2007) also concluded that, for experiments at high pressures, the presence of CO₂ reduced the rate of C-H₂O reaction.

In Eq. (1), the structure function $f(X)$ represents the reactive surface of the particle. Its evolution during the gasification or the combustion reactions is difficult to predict and is subject to discussion in the literature (Mermoud et al., 2006). Due to the complex char structure, several kinetic models are reported to represent the structure function. Table 1 shows that the most commonly models used to represent the char gasification kinetic are the Volumetric Model (VM) (Marquez-Montesinos

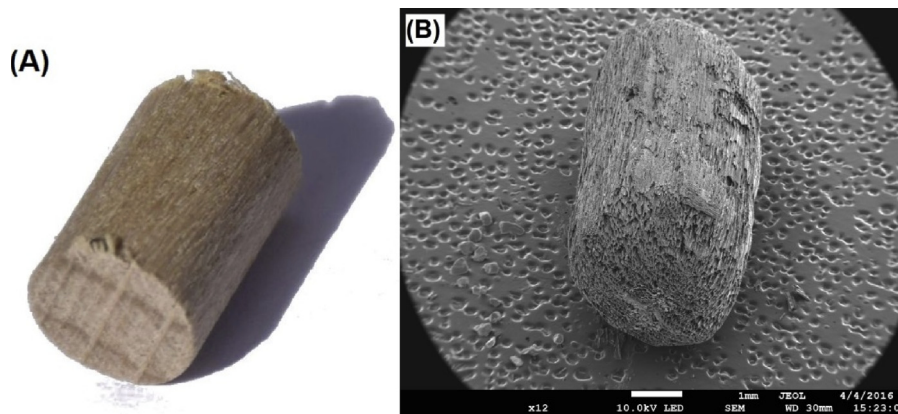


Fig. 1 – (A) beech stick particle (STI), (B) char (STI650) obtained by pyrolysis of beech stick at 650 °C in a fluidized bed reactor.

Table 2 – Proximate analysis of the beech stick (wt%, dry basis).

Biomass	Moisture (%)	Volatile matters (%)	Fixed carbon ^a (%)	Ash (%)
Beech stick	8.40	76.7	14.7	0.2

^a By difference.

Table 3 – Ultimate analysis and properties of the different solids.

Material	STI	STI650	Olivine
Composition (db,wt.%)	C: 44.63 H: 6.37 O: 45.24 Ash: 0.2	C: 84.47 H: 2.75 O: 7.39 Ash: 5.39	MgO: 57.5–50.0 SiO ₂ : 39.0–42.0 CaO: max 0.4 Fe ₂ O ₃ : 8.0–10.5
Chemical formula	CH _{1.71} O _{0.76}	CH _{0.39} O _{0.07}	(Mg _{1-x} Fe _x) ₂ SiO ₄
d ₃₂ (μm)	–	–	264
Apparent density ρ _a (kg m ⁻³)	718 ± 24	212 ± 32	2965 ± 20
True density ρ _{t,c} (kg m ⁻³)	1362.5 ± 1	1589.4 ± 5	3265 ± 2
Solid porosity ε _p (-)	0.47	0.87	0.09
U _{mf} (850 °C) (cm s ⁻¹)	–	–	5.8

db: dry basis.

et al., 2002; Nandi and Onischak, 1985; Bhat et al., 2001; Groeneveld and van Swaaij, 1980; Zhai et al., 2015; Barrio et al., 2001; Kojima et al., 1993; Hémati and Laguerie, 1988), the Shrinking Core Model (SCM) (Le and Kolaczowski, 2015; Zhai et al., 2015) and the Random Pore Model (RPM) (Paviet et al., 2007; Ahmed and Gupta, 2011; Woodruff and Weimer, 2013). The Volumetric Model (Dutta and Wen, 1977) assumes a homogeneous reaction throughout the particle while the Shrinking Core Model (Wen, 1968) considers a reaction front onto the char surface which moves within the particle. These two models (i.e. VM and SCM) describe a decrease in the reaction rate with conversion. The Random Pore Model developed by Bathia and Perlmutter (1980) attempts to describe the change in the pores structure during char conversion. This model introduces a structural parameter by considering that the char particle is porous and the reaction occurs at the internal surface of the pores. As the reaction proceeds, a random overlapping of the pores occurs which can increase or reduce the reactive surface area. This model was largely used for char gasification due to its ability to predict a bell-shape relationship between the reaction rate and the conversion rate which is often observed during gasification experiments. Finally, some authors (Kramb et al., 2014; Nilsson et al., 2012; Septien et al., 2015) also represented the structure function with an empirical expression valid for a specific range of operating conditions.

The present study investigates the isothermal kinetic of beech char gasification with steam in a fluidized bed reactor and at atmospheric pressure. This char was obtained from fast pyrolysis of beech stick at 650 °C in an annex fluidized bed reactor. The paper systematically studies the influence of temperature between 700 and 850 °C, steam partial pressure between 0.3 and 0.7 bars and hydrogen partial pressure in the range of 0.1–0.25 bars on both the production of non-condensable gases

and on the gasification rate. The effect of hydrogen partial pressure on the CH₄ production is also examined in order to highlight the potential interactions between carbon and H₂ during the steam gasification. Finally, a kinetic model is also proposed to represent the experimental data.

2. Experimental section

2.1. Char preparation

The biomass is a cylindrical beech stick (D = 6 mm, L = 10 mm). A picture of the raw materials is given in Fig. 1(A). The proximate analysis of this fuel was carried out following the standard test method for chemical analysis of wood charcoal D 1762-84. The results are given in Table 2.

The pyrolysis procedure can be found in detail in a previous work (Morin et al., 2016). Briefly, beech sticks were pyrolyzed in an annex batch fluidized bed reactor at 650 °C with a heating rate of 18 °C/s. The pyrolysis was conducted at atmospheric pressure under an inert atmosphere of nitrogen. After reaching the temperature of 650 °C and a steady state regime in the reactor, about 20 g of biomass were introduced in the hot fluidized bed of sand particles. This step was repeated several times to produce a sufficient amount of char. After the pyrolysis, the produced chars (called STI650) were cooled under a flow of nitrogen before being recovered the day after by sieving. A picture of the obtained char is given in Fig. 1(B).

The physical and chemical properties of the beech stick and STI650 are summarized in Table 3. The apparent density of the biomass and char was measured from the weight and volume of five single particles. The true density was obtained by helium pycnometry. The porosity of the different solids was determined using the following expression:

$$\varepsilon_p = 1 - \frac{\rho_a}{\rho_{t,c}} \quad (7)$$

2.2. Char gasification with steam in a fluidized bed reactor

2.2.1. Experimental setup

The steam gasification of STI650 was carried out in a fluidized bed reactor. The experimental setup is shown in Fig. 2 and has already been described in a previous paper (Morin et al., 2018). The reactor can be supplied with nitrogen, steam and hydrogen at different proportions according to the gasification operating conditions. N₂ and H₂ mass flow rates are carefully regulated by two mass flowmeters Aera FC-7700-CD. H₂O is fed by a pump Gilson 305 100SC in liquid form. The feeding gases are preheated between 200 and 300 °C in a stainless steel tube (inner diameter of 1 cm) forming a coil around the reactor. The coil is fed with liquid water which is continuously vaporized. Olivine particles are used as fluidized medium. The physicochemical properties of olivine are given in Table 3. The minimum fluidization velocity of this solid was measured experimentally (i.e. pressure drop of the bed and standard deviation of pressure fluctuations versus gas velocity) and is equal to 5.8 cm/s at 850 °C.

The temperature inside the fluidized bed is controlled by two thermocouples located at 5 and 25 cm above the distributor while a differential pressure transmitter connected at 5 and 500 mm above the distributor follows the pressure drop of the bed.

After reaching the gasification operating conditions and a steady-state regime, a well-known amount of char (8.7 g) is introduced from the top of the reactor and directly falls down to the top of the hot fluidized bed.

2.2.2. Sampling method and gas analysis

A stainless steel mobile probe (inner diameter of 4 mm) located at the fluidized bed surface is used to continuously sample the produced gas. The gas is sucked by a vacuum pump with a constant volume flow rate of 100 mL min⁻¹ at STP. At the mobile probe outlet, the pumped gas passes through a cyclone to separate gas from particles before entering a Gas Chromatograph (GC). This analyzer quantifies the potential presence of tars during the experiments. This GC is equipped with a Varian CP-Porabond Q 25 m × 0.32 mm column heated from 120 °C to 300 °C at 20 °C/min. A Flame Ionization Detector (FID) enables the quantification of benzene, toluene, phenol and naphthalene. At the GC outlet, the gas passes through two wash-bottles cooled at 0 °C and -20 °C respectively to remove any traces of water and tars. To prevent any condensations of steam, all of the lines from the reactor to the entrance of the condensation system are heated to a temperature of 150 °C.

Finally, a micro Gas Chromatograph (micro GC) Agilent 490 is used to online analyze the non-condensable gases. It is equipped with a Poraplot U 10 m × 0.25 mm ID column connected to a Thermal Conductivity Detector calibrated for CO₂ and C₂H_x quantification. A CP-Molsieve 5A 10 m × 0.25 mm column connected to a TCD is calibrated for the analyses

Table 4 – Operating conditions of each experiment, (solid medium: olivine, U_g = 2.5 · U_{mf}).

Experiments	P _{N₂} (bar)	P _{H₂O} (bar)	P _{H₂} (bar)	Temp. (°C)
Dev_1a	1	0	0	700
Dev_1b	1	0	0	750
Dev_1c	1	0	0	800
Dev_1d	1	0	0	850
Dev_1a_G_2	0.7	0.3	0	700
Dev_1b_G_2	0.7	0.3	0	750
Dev_1c_G_2	0.7	0.3	0	800
Hyd_3a	0.9	0	0.1	850
Hyd_3b	0.8	0	0.2	850
G_4a	0.7	0.3	0	700
G_4b	0.7	0.3	0	750
G_4c	0.7	0.3	0	800
G_4d	0.7	0.3	0	850
G_5a	0.9	0.1	0	850
G_5b	0.7	0.3	0	850
G_5c	0.5	0.5	0	850
G_5d	0.3	0.7	0	850
G_6a	0.7	0.3	0	850
G_6b	0.6	0.3	0.1	850
G_6c	0.55	0.3	0.15	850
G_6d	0.45	0.3	0.25	850

and quantification of N₂, H₂, O₂, CO and CH₄. The time-lapse between two quantifications is 3 min.

A previous paper (Morin et al., 2018) showed that the sampling gas method in the fluidized bed reactor strongly influences the evolution of the molar percentages of the detected gases versus time due to gas mixing in the sampling system (probe, cyclone, lines and wash-bottles). This effect was highlighted by observing the response of the sampling gas lines to a hydrogen concentration step at the entrance of the reactor. It was found that the variation in the molar percentage of hydrogen measured by the micro GC versus time can be well represented by the association of 5 continuous flow stirred-tank reactors with a residence time of 1.69 min each. These 5 reactors in series represent the transfer function of the sampling gas lines and will be considered in the kinetic modelling.

2.2.3. Operating conditions and data treatment

Tests were conducted at atmospheric pressure in the presence of olivine particles. For each experiment, the gas velocity in the reactor was set to 2.5 times the minimum fluidization velocity so that any particles entrainment is avoided and a homogeneous temperature and a fairly good mixing between char and olivine is obtained (Morin et al., 2018). The amount of char introduced in the reactor is fixed to 8.7 g which corresponds to 1.5% of the total mass of the bed. After each gasification experiment, the carbon balance was checked and was close to 100% ± 5%.

The different authors in the literature (Di Blasi, 2009; Bhat et al., 2001) agreed that the kinetic of char gasification with steam takes place in Regime I for temperatures up to 900 °C. Therefore, in this work, the gasification experiments are performed for temperatures between 700 and 850 °C.

The different operating conditions of each experiment are presented in Table 4.

- Experiments “Dev_1” study the effect of temperature on the thermal degradation of char just after its introduction in

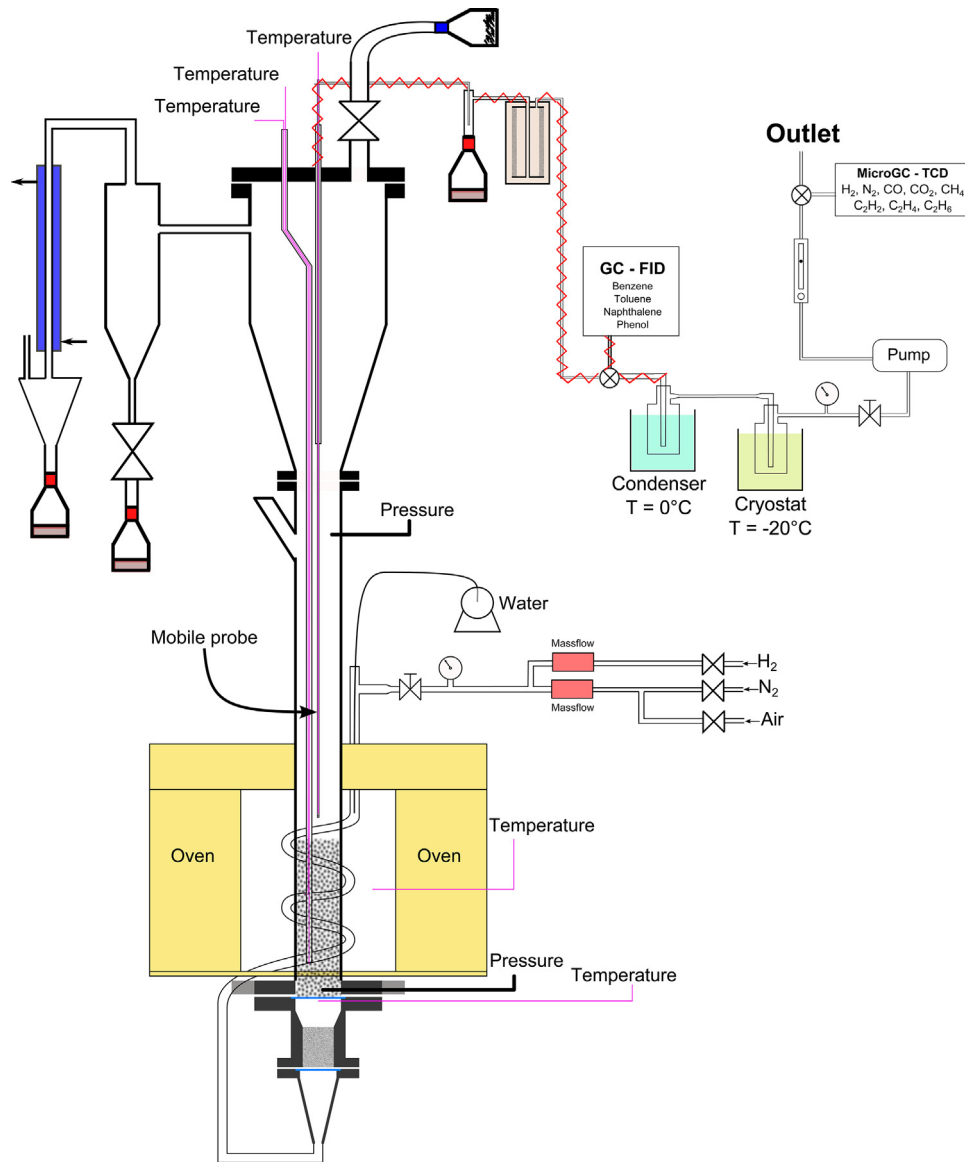


Fig. 2 – Experimental setup used for the char gasification in a fluidized bed reactor.

the reactor. These tests are performed for temperatures between 700 and 850 °C and a pure flow of nitrogen.

- The set of experiments “Dev.1.G.2” carries out the thermal degradation of char under pure N₂ followed by the steam gasification of the carbonaceous residue at three different temperatures (700, 750 and 800 °C) and a constant steam partial pressure of 0.3 bar.
- Tests “Hyd.3” investigate the effect of hydrogen partial pressure between 0.1 and 0.2 bars in a gas mixture of H₂ and N₂ at 850 °C on the CH₄ production and the char conversion.
- Experiments “G.4” study the effect of temperature between 700 and 850 °C on the steam gasification of STI650 for a constant steam partial pressure of 0.3 bars.
- The set of tests “G.5” investigates the effect of steam partial pressure between 0.1 and 0.7 bars on the steam gasification of STI650 at 850 °C.
- Finally, experiments “G.6” study the influence of hydrogen partial pressure between 0.1 and 0.25 bars during the steam gasification of STI650 at 850 °C and a constant steam partial pressure of 0.3 bars.

For each experiment, the composition of the non-condensable gases was analyzed as a function of time from the

continuous micro GC analyses. The nitrogen is not involved during the gasification reaction and is only used as an inert gas for mass balances. The total molar flow rate at the reactor outlet is given by:

$$\dot{n}_t(t) = \frac{\dot{n}_{N_2}}{x_{N_2}(t)} \quad (8)$$

where $\dot{n}_t(t)$ is the instantaneous total molar flow rate (mol min⁻¹), \dot{n}_{N_2} represents the molar flow rate of nitrogen at the entrance of the reactor (mol min⁻¹) and $x_{N_2}(t)$ is the measured molar fraction of nitrogen at the reactor outlet.

The molar flow rate of each component is calculated as follows:

$$\dot{n}_i(t) = x_i(t) \cdot \dot{n}_t(t) \quad (9)$$

where $\dot{n}_i(t)$ and $x_i(t)$ are the instantaneous molar flow rate and molar fraction of component *i*, respectively. During the char devolatilization and gasification, H₂, CO, CO₂, CH₄ and traces of C₂H_x were detected by the gas analyzer. It is important to note that no tars (i.e. benzene, toluene, phenol and naphthalene) were detected during any experiments.

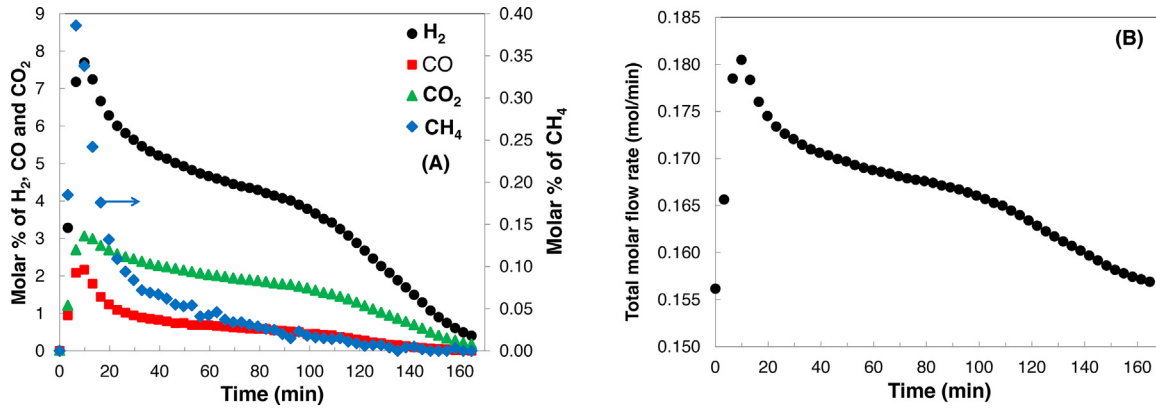


Fig. 3 – (A) Molar percentages of the non-condensable gases versus time, (B) total molar flow rates versus time, (experiment G.4c, $\dot{n}_{N_2} = 0.155 \text{ mol min}^{-1}$).

The cumulative amount of each component produced during a time “t” is defined according to the following expression:

$$n_i(t) = \int_{t=0}^t \dot{n}_i(t) dt \quad (10)$$

where $n_i(t)$ is the cumulative amount of component i during the time t.

The carbon molar flow rate is calculated according to the following expression:

$$\dot{n}_{carbon}(t) = \sum_{i=1}^{N_{tot}} \dot{n}_i(t) \cdot \gamma_i \quad (11)$$

where $\dot{n}_{carbon}(t)$ is the carbon molar flow rate ($\text{mol} \cdot \text{min}^{-1}$) and γ_i represents the number of carbons in the component i.

The carbon conversion rate is determined by:

$$X_c = \frac{\int_{t=0}^t \dot{n}_{carbon}(t) dt}{(n_{carbon})_{char}} \quad (12)$$

where $(n_{carbon})_{char}$ is the amount of introduced carbon in the reactor (mol).

The instantaneous gasification rate is obtained using the equation:

$$\frac{dX_c}{dt} = \frac{\dot{n}_{carbon}(t)}{(n_{carbon})_{char}} \quad (13)$$

Finally, the apparent reaction rate is defined as the derivative of the evolution of the carbon conversion rate versus time, for a conversion rate of 40%:

$$R_{app} = \left. \frac{dX_c}{dt} \right|_{X_c=0.4} \quad (14)$$

2.2.4. Experimental measurement errors

Experimental errors were estimated from the gas analyzer calibration and the accuracy of both the gas mass flowmeters and the char mass introduced in the reactor during the combustion. For each gas analysis, the measured values are within an accuracy of 1% with a confidence level of 95%. Consequently, an experimental error of 1% was taken for components quantification. The mass flowmeters accuracy was fixed to 0.5% of full scale. Regarding the char mass measurement accuracy, the systematic constant error is equal to 0.1 g. Hence, in the fol-

lowing, from these three systematic experimental errors, the error bars are introduced into the experimental data.

Besides, some experiments (i.e. gasification at 850 °C with $P_{H_2O} = 0.3$ bars and $P_{H_2} = 0$ bar) have been repeated with a time lapse of 5 months. The results showed a very good repeatability of the replicate experimental measurements.

3. Results & discussions

3.1. Typical experiment

In this section, the results of a typical experiment (i.e. experiment G.4c) are presented and the different findings can be generalized to any other tests.

The results of the steam gasification of STI650 at 800 °C and a steam partial pressure of 0.3 bars (experiment G.4c) are given in Fig. 3. Fig. 3(A) presents the molar percentages variation of the produced gases H₂, CO, CO₂ and CH₄ with time. The nitrogen molar percentage is not shown since it only acts as an inert gas. It can be seen that the molar percentage of each component substantially increases before reaching a maximum followed by a gradual decrease to zero. Fig. 3 (B) shows the total molar flow rate of the produced gas. Therefore, the combination of results given in Fig. 3(A) and (B) enables the partial molar flow rates of each component to be calculated.

It can also be observed that H₂ is the larger produced component during the steam gasification of char. A large amount of CO and CO₂ is also produced while a non-negligible amount of CH₄ is formed.

Fig. 4 shows the instantaneous gasification rate (Eq. (13)) versus carbon conversion rate during the experiment G.4c. The curve profile emphasizes that the reaction rate first increases, reaches a maximum (for $X_c = 0.1$) followed by a decrease to zero. Besides, the decrease in the reaction rate occurs in two stages: from $X_c = 0.1$ to $X_c = 0.9$, it is related to the char consumption which progressively decreases the formation of volatile products; for X_c higher than 0.9, it corresponds to the end of the reaction.

Three different points of view can be found in the literature to explain the maximum reaction rate which is frequently observed during the char gasification (Paviet et al., 2007; Ahmed and Gupta, 2011; Kramb et al., 2014; Nilsson et al., 2012; Woodruff and Weimer, 2013):

- First, some authors (Paviet et al., 2007; Ahmed and Gupta, 2011; Kramb et al., 2014; Nilsson et al., 2012; Woodruff and Weimer, 2013) attributed the maximum reaction rate to a

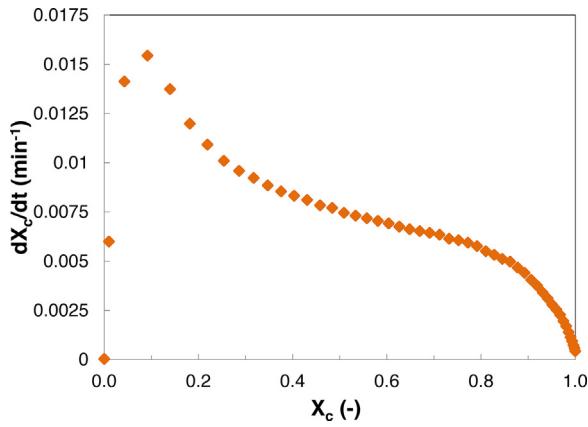


Fig. 4 – Instantaneous gasification rate versus carbon conversion rate, (experiment G.4c).

change of the char reactive surface during the gasification. Hence, they represent the gasification rate using the Random Pore Model (RPM) proposed by Bathia and Perlmutter (1980). This model considers two competing effects of structural change in the porous char particle. As the reaction proceeds, the char reactive surface area may either increase related to pores growth or decrease due to pores intersection and coalescence. The gasification rate reaches a maximum when the second effect overshadows the first effect.

- For isothermal gasification tests in TGA or fixed bed reactor, most of the authors (Barrio et al., 2001) employed a switching gas method which consists in heating the reactor under an inert atmosphere to the desired temperature before switching the gas from inert to reactive to perform the char gasification. In this case, the reaction rate profile at the beginning of the experiment is attributed to the low gasification agent content in the reactive atmosphere. For example, in a previous work on char combustion (Morin et al., 2017), it was found that it requires about 25 min for the reactive gas to completely replace the inert gas just after switching the gas from inert to reactive in the TGA. This time leads to a non-constant steam partial pressure at the beginning of the gasification which is responsible for the maximum gasification rate.
- Finally, for char gasification experiments in which the produced gases are continuously sampled and analyzed (Nilsson et al., 2014, 2012), the maximum reaction rate may be attributed to the gas mixing in the sampling lines. This phenomenon lowers the amount of detected gas and affects the kinetic of char gasification. This effect can be corrected using several continuous flow stirred-tank reactors in series as indicated in Section 2.2.2.

In our experiments, since the char is directly introduced in the reactor once a steady state is reached (i.e. a constant temperature and steam partial pressure), the strong increase in the instantaneous gasification rate to reach a maximum may be the combination of two different phenomena: the gas mixing in the sampling lines as well as the thermal degradation (devolatilization) of char just after its introduction in the reactor. This char devolatilization step produces a significant amount of H₂, CO, CO₂ and CH₄ at the initial stage of the char gasification.

Fig. 5(A) shows the molar percentages of H₂, CO, CO₂ and CH₄ without considering the presence of nitrogen in the product gas versus the carbon conversion rate. The molar per-

centages of CO+CO₂ is also presented in this figure. Three zones can be emphasized:

- (1) For $X_c < 0.1$, the molar percentages of H₂, CO and CO₂ strongly increase. This initial raise is associated with the char devolatilization step which produces large amounts of non-condensable gases.
- (2) For a carbon conversion rate between 0.1 and 0.95, the molar percentages reach a constant value. This plateau is attributed to the effect of both the steam gasification reaction (Reaction (I)) and the Water-Gas-Shift reaction (Reaction (II)).
- (3) For $X_c > 0.95$, the molar percentages gradually decrease to zero which is related to the end of the char gasification.

The steps (1) and (2) can also be highlighted by introducing a parameter θ which is defined according to the molar flow rates of H₂, CO and CO₂ as follows:

$$\theta = \frac{\dot{n}_{H_2}}{\dot{n}_{CO} + 2 \cdot \dot{n}_{CO_2}} \quad (15)$$

This parameter emphasizes the effect of both the steam gasification and the WGS reactions during the experiment G.4c. When $\theta = 1$, it can be assumed that both Reactions (I) and (II) are predominant. This result is developed in Appendix A.

Fig. 5(B) shows the profile of the parameter θ versus the conversion rate. It can be seen that θ strongly increases for $X_c < 0.15$ before reaching a constant value equal to 1. This confirms that, during the char gasification with steam, the reaction occurs in two stages: the char devolatilization followed by the steam gasification according to Reactions (I) and (II). Besides, from these results, it can be assumed that the Boudouard reaction (i.e. Reaction (III)) can be neglected during steam gasification experiments.

Fig. 5(A) also shows that a non-negligible amount of CH₄ is produced. The molar percentage of this component first substantially increases before progressively decreasing. The origin of its formation is discussed in Section 3.3.

3.1.1. Effect of char devolatilization on the steam gasification

A second set of tests (i.e. experiments Dev.1.G.2) was performed in order to emphasize the effect of the char devolatilization step during the steam gasification. The experiments include two stages: the devolatilization of STI650 under pure nitrogen and the successive steam gasification of the residue from the devolatilization step. The experimental protocol consists in heating the fluidized bed to 800 °C under an inert atmosphere of nitrogen. Once a steady state regime is reached, the char is introduced in the reactor. The char devolatilization takes place for about 40 min. The instantaneous reaction rate of the devolatilization step is plotted versus time on the left side of Fig. 6. After the char devolatilization, the gas is switched from nitrogen to a mixture of N₂/H₂O ($P_{H_2O} = 0.3$ bars) to perform the steam gasification. The comparison between the instantaneous gasification rate obtained after the char devolatilization step and the one obtained from direct steam gasification of STI650 is also presented in Fig. 6. For better comparison of the results, the beginning of the direct steam gasification has been shifted to 40 min. A strong difference in reactivity is observed at the beginning of the steam gasification. Indeed, between 40 and 60 min in Fig. 6, the instantaneous reaction rate is higher for the direct gasi-

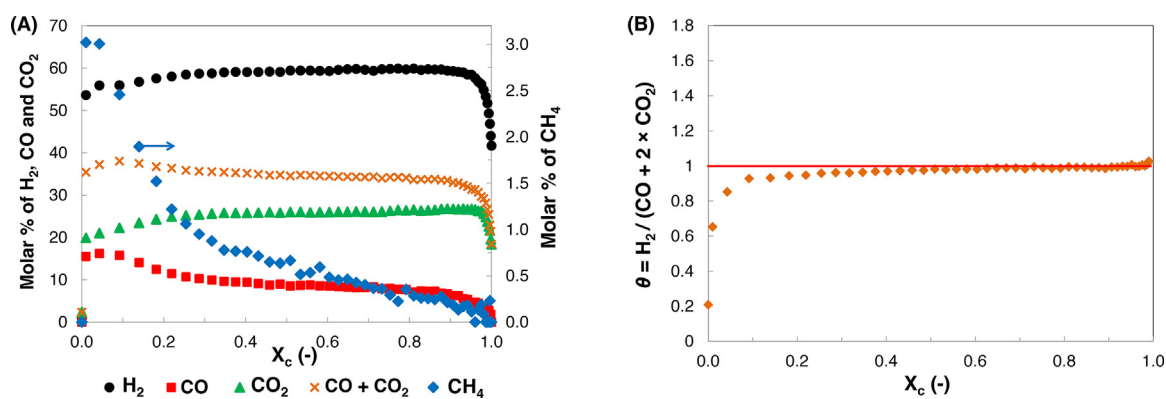


Fig. 5 – (A) Molar percentages of the non-condensable gases without considering nitrogen in the product gas, (B) parameter θ versus conversion rate, (experiment G_4c).

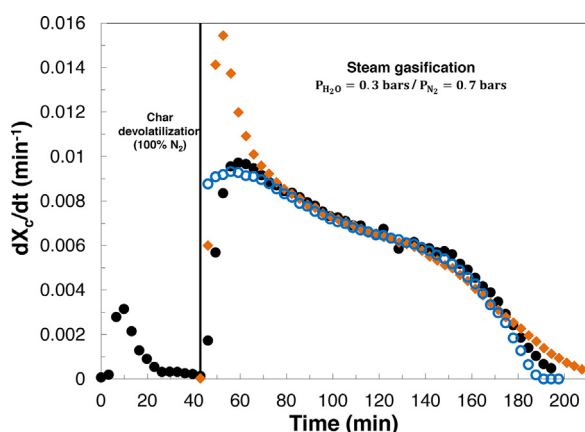


Fig. 6 – Instantaneous reaction rate versus time, (●) char devolatilization followed by steam gasification (experiment Dev_1c.G_2), (◆) direct steam gasification (experiment G_4c), (○) intrinsic gasification rate (experiment Dev_1c.G_2).

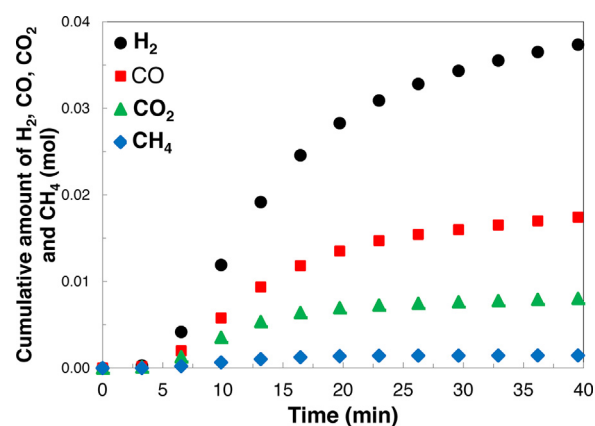


Fig. 7 – Cumulative amount of the different components produced during the devolatilization of STI650, (experiment Dev_1c).

fication of STI650 compared to that of the gasification of the carbonaceous residue obtained after the devolatilization step. Besides, the presence of steam seems to have an effect on the char devolatilization step as the strong increase in the instantaneous gasification rate during the direct steam gasification is more acute than the one of devolatilization.

3.1.2. Effect of the transfer function on the steam gasification

Fig. 6 also presents experimental results of the char steam gasification after the devolatilization step corrected by the transfer function of the sampling gas system (○). It is observed that the strong increase in the instantaneous reaction rate is significantly attenuated by removing the effect of gas mixing in the sampling lines. After 40 min of reaction, no differences are observed between the two curves which indicate that the transfer function has a strong influence at the beginning of the char gasification.

3.2. Effect of temperature on char devolatilization step (experiments Dev_1)

In a previous work (Morin et al., 2016), it was shown that STI650 is a complex solid residue which contains both aromatic and amorphous carbon. The amorphous carbon represents the non-aromatic carbons (i.e. aliphatic, carbonyl, methoxyl groups) trapped in the char macromolecules. Hence, during a rapid heat treatment, the amorphous carbon is released

as volatile products (H₂, CO, CO₂ and CH₄). This leads to a change in the physicochemical properties of char which becomes more aromatic with a higher carbon content. This char devolatilization step was also reported by some authors in the literature (Klinghoffer et al., 2012). For instance, in the case of char devolatilization in TGA under pure nitrogen, Klinghoffer et al. (2012) observed a mass loss which was attributed to the loss of volatile products that are still present in the char.

In this work, the char devolatilization step was highlighted by analyzing the formation of non-condensable gases during the insertion of STI650 in the reactor in the presence of pure nitrogen. Fig. 7 presents the cumulative amount of the non-condensable gases produced during the char devolatilization at 800 °C (experiment Dev_1c). It can be seen that a non-negligible amount of H₂, CO, CO₂ and CH₄ is produced. These gases are the results of the decomposition of the carbon-oxygen and carbon-hydrogen matrix to form CO, CO₂ and CH₄. Besides, it was found that H₂ is the higher produced component followed by CO, CO₂ and CH₄.

Fig. 8(A) highlights that an increase in the devolatilization temperature leads to a raise of the cumulative amount of H₂ in the product gas. This phenomenon was also observed for CO and CH₄. However, it was found that the temperature has no influence on the amount of CO₂. The influence of temperature on the char conversion rate is shown in Fig. 8(B). The devolatilization step lasts approximately 40 min and a conversion less than 5% is reached. Moreover, a higher temperature yields to a higher partial conversion of the char. From

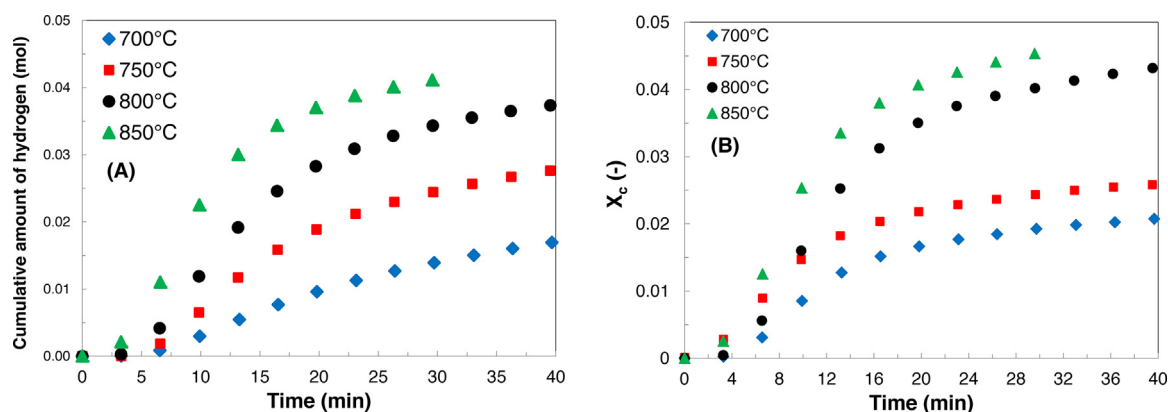


Fig. 8 – (A) Effect of the temperature on the cumulative amount of hydrogen in the product gas, (B) effect of the temperature on the carbon conversion rate, (experiments Dev_1).

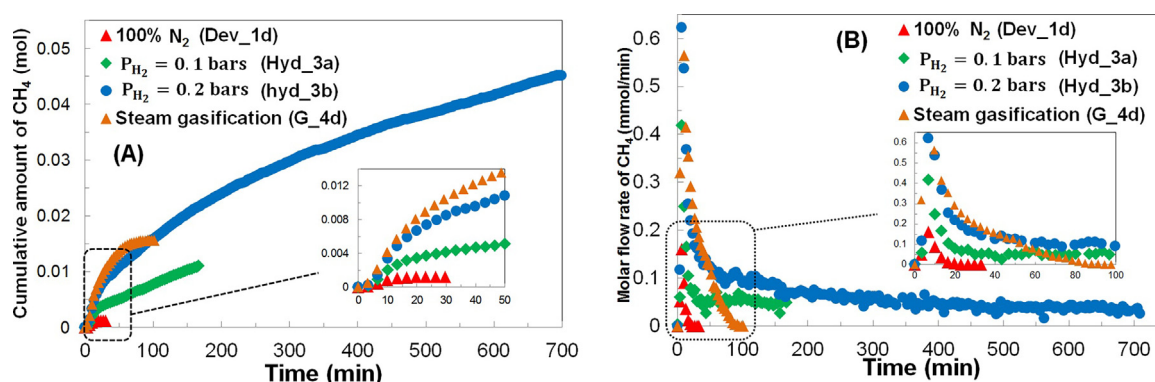


Fig. 9 – Effect of hydrogen partial pressure on (A) the cumulative amount of CH₄ (B) the molar flow rate of CH₄ (experiments Dev_1d, Hyd_3 and G_4d).

Table 5 – Effect of temperature on the chemical formula of the residual carbonaceous solid obtained after the devolatilization of STI650.

Temperature (°C)	CH _m O _p
STI650	CH _{0.39} O _{0.07}
700	CH _{0.36} O _{0.05}
750	CH _{0.33} O _{0.05}
800	CH _{0.31} O _{0.04}
850	CH _{0.30} O _{0.03}

the mass balance on carbon, hydrogen and oxygen, the effect of temperature on the char composition was evaluated. The results are presented in Table 5 which highlights that a higher devolatilization temperature leads to: a higher partial degradation of char, a lower amount of hydrogen and oxygen in the residual carbonaceous solid.

3.3. Interactions between char and hydrogen (experiments Hyd_3)

During the steam gasification of STI650, a non-negligible amount of methane is detected for each temperature and steam partial pressure. In the literature, the production of CH₄ during the char gasification at atmospheric pressure is not well-understood yet and is usually neglected (Blackwood and McGrory, 1958). Indeed, the reaction between carbon and hydrogen is not thermodynamically favored at low pressures and high temperatures. Therefore, it may be questionable whether this reaction occurs during the steam gasification and is responsible for the CH₄ production. In the literature,

it was mainly investigated at elevated pressures (Liu et al., 2017) while a very few studies gave data at atmospheric pressure (González et al., 2002). Bibliographic works also showed that alkali and alkaline earth metals as well as Fe and Ni may catalyze the reaction between char and H₂ (Liu et al., 2017; González et al., 2002).

This section aims to establish the effect of hydrogen partial pressure on the char-hydrogen interactions and the CH₄ production. A set of experiments was performed in the fluidized bed reactor (experiments Hyd_3) at 850 °C in a gas mixture of H₂ and N₂ and at atmospheric pressure. The effect of hydrogen partial pressure was investigated up to 0.2 bars. Apart from the char devolatilization step (i.e. during the first 40 min of the reaction), CH₄ was the main produced gas detected during the experiments.

Fig. 9 shows both the cumulative amount and the molar flow rate of CH₄ versus time for various hydrogen partial pressures. Results from the char steam gasification for a steam partial pressure of 0.3 bars (experiment G_4d) are also presented in this figure.

Several observations can be made:

- For each hydrogen partial pressure, the cumulative amount of methane continuously increases during the experiment (Fig. 9(A)) which highlights that the reaction between char and hydrogen is very low. Indeed, it was also found that, in the case of a hydrogen partial pressure equal to 0.2 bars, a conversion rate of about 11% is obtained after 700 min of reaction.

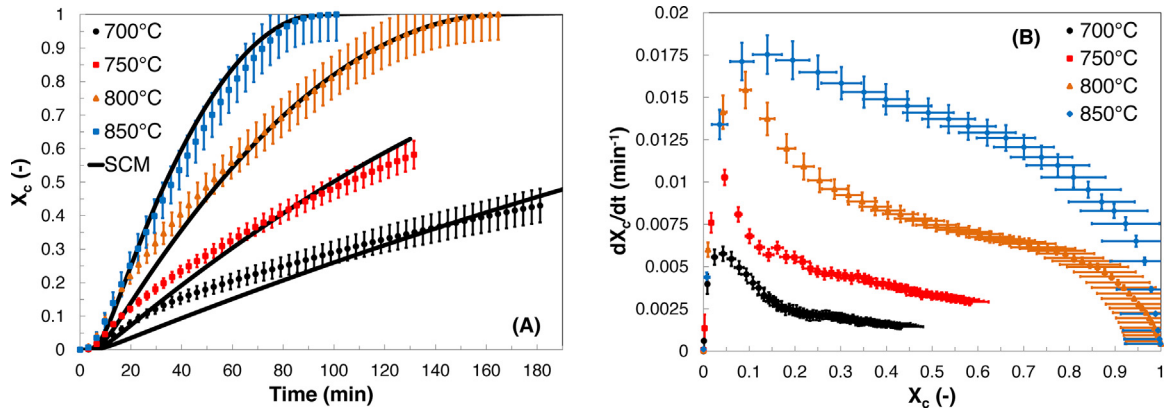


Fig. 10 – Effect of temperature on the (A) conversion rate versus time, (B) instantaneous gasification rate versus conversion rate, (experiments G.4).

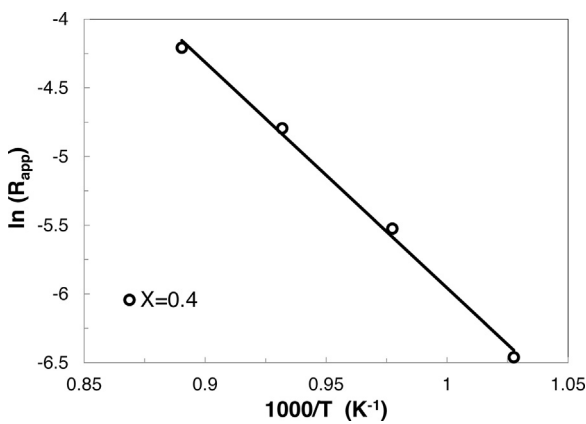


Fig. 11 – Logarithm of the apparent reaction rate versus $1/T$ during the char gasification, (experiments G.4).

- The formation of CH_4 in the product gas increases by raising the hydrogen partial pressure (Fig. 9(A)).
- The molar flow rate of CH_4 substantially increases at the beginning of the reaction before gradually decreasing (Fig. 9(B)). This strong peak is the results of the char devolatilization just after its introduction in the reactor. This devolatilization step is much faster than the reaction between char and hydrogen.
- During the steam gasification of char, both the cumulative amount and the molar flow rate of CH_4 are higher compared to those obtained during the char devolatilization. These

results can be explained by the interactions at the solid surface between the hydrogen produced during the gasification and the reactive char.

- During the steam gasification of char, for carbon conversion rates less than 95% (i.e. a reaction time less than 75 min), the cumulative amount of CH_4 is slightly higher than the one obtained with a hydrogen partial pressure of 0.2 bars. Therefore, it seems that the produced hydrogen from the char gasification gives rise to more interactions at the char surface and a higher CH_4 production.

Consequently, these results showed that, despite the thermodynamic limitations of char- H_2 reaction at atmospheric pressure, it can be assumed that interactions between carbon and hydrogen occur in the reactor. The reaction is very slow and may explain the formation of methane during the steam gasification of char.

3.4. Direct steam gasification

3.4.1. Effect of temperature (experiment G.4)

Fig. 10(A) presents the effect of gasification temperature between 700 and 850 °C on the conversion rate versus time under a constant steam partial pressure of 0.3 bars. As the temperature is increased, the steam gasification of char becomes faster. This result is well-known in the literature (Nandi and Onischak, 1985; Bhat et al., 2001; Klose and Wölki, 2005; Paviet et al., 2007; Groeneveld and van Swaaij, 1980; Ahmed and Gupta, 2011; Nilsson et al., 2014, 2012; Le and

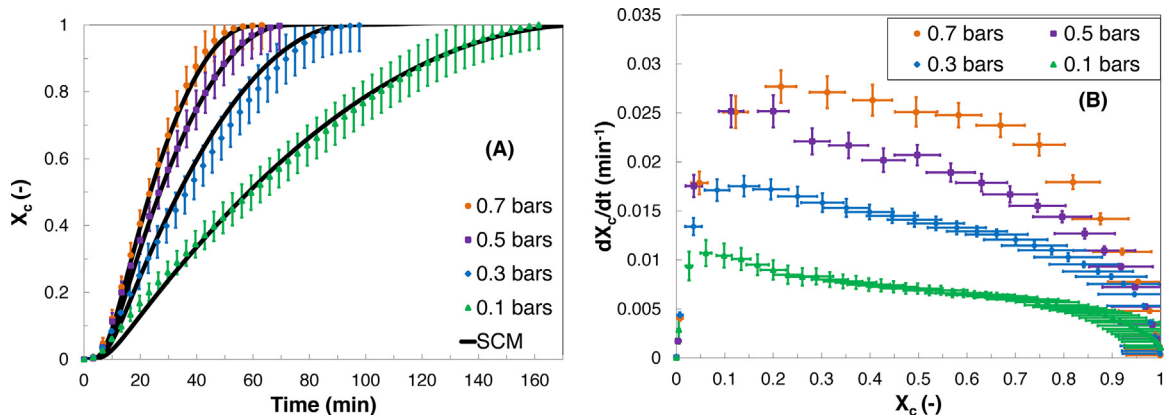


Fig. 12 – Effect of steam partial pressure on the (A) conversion rate versus time, (B) instantaneous gasification rate versus conversion rate, (experiments G.5).

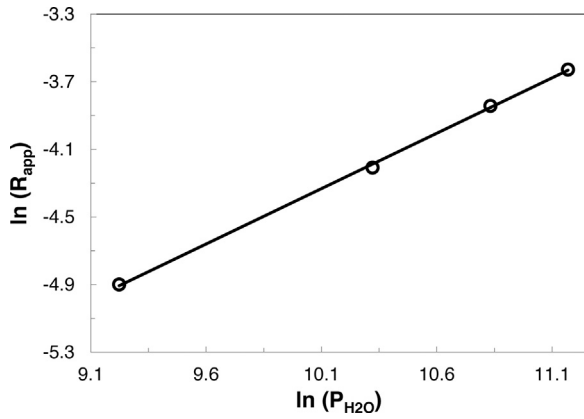


Fig. 13 – Logarithm of the apparent reaction rate versus logarithm of steam partial pressure at 850 °C, (experiments G.5).

Kolaczowski, 2015; Kramb et al., 2014; Zhai et al., 2015; Barrio et al., 2001; Kojima et al., 1993; Hawley et al., 1983; Hémati and Laguerie, 1988; Woodruff and Weimer, 2013). For instance, it requires 29.3 min, 39.5 min, 78.8 min and 161.2 min to reach a conversion rate of 0.4, for temperatures of 850 °C, 800 °C, 750 °C and 700 °C, respectively.

Fig. 10(B) illustrates the effect of temperature on the instantaneous gasification rate versus conversion. For each experiment, the profile curves increase, reach a maximum before gradually decreasing to zero. As mentioned in Section 3.1, this profile is the result of both the gas mixing in the sampling lines and the char devolatilization step.

Fig. 11 shows that gasification experiments are very well correlated to a linear expression between the logarithm of apparent reaction rate (Eq. (14)) and $1/T$. This indicates that the apparent reaction rate can be well represented by an Arrhenius law. From Eqs. (1) and (2) and the slope of the straight line, it is possible to determine the activation energy without considering any reaction models. Its value is equal to 137 kJ mol^{-1} and is in the same order of magnitude than previous works in the literature (E_a comprised between 96 and 275 kJ mol^{-1} , see Table 1).

3.4.2. Effect of steam partial pressure (experiments G.5)

The influence of steam partial pressure was conducted between 0.1 and 0.7 bars at 850 °C. The results show that a raise of the steam partial pressure leads to a higher gasification rate and a faster char conversion (Fig. 12).

Fig. 13 presents the logarithm of apparent reaction rate versus the logarithm of steam partial pressure at 850 °C. Again, considering Eqs. (1) and (2) and from the slope of the straight line, the reaction order with respect to steam can be determined without considering any reaction models. Its value is equal to 0.66 which is close to values obtained in the literature (n comprised between 0.33 to 0.75, see Table 1).

3.4.3. Effect of hydrogen partial pressure (experiments G.6)

This section investigates the effect of hydrogen partial pressure between 0.1 and 0.25 bars during the steam gasification of char at 850 °C with a constant steam partial pressure of 0.3 bars (experiments G.6).

Fig. 14(A) presents the effect of hydrogen partial pressure on the instantaneous gasification rate versus conversion rate during the steam gasification of char (experiments G.6). It can be seen that the presence of hydrogen inhibits the reaction

of char gasification with steam. The effect of H_2 was found to be significant for hydrogen partial pressures higher than 0.15 bars. Besides, the results have shown that the produced molar flow rates of H_2 and CO_2 decrease by raising the hydrogen partial pressure. This is due to Reactions (I) and (II) being favored in the indirect direction. On the contrary, the amount of CH_4 strongly increases with the hydrogen partial pressure. As mentioned in Section 3.3, an increase in the hydrogen partial pressure promotes the interactions between char and H_2 and favors the CH_4 production. Finally, the molar flow rate of CO was found to increase by raising the hydrogen partial pressure up to 0.15 bars and decrease for higher pressures. It is attributed to the competition between Reactions (I)–(III). These results are highlighted in Fig. 14 (B) which plots the molar flow rates of H_2 , CO , CO_2 and CH_4 versus hydrogen partial pressure for a given conversion rate of 0.4. Moreover, it seems that the hydrogen partial pressure up to 0.15 bars has a higher effect on the WGS reaction while for higher partial pressures, it mainly influence the steam gasification of carbon.

In the literature, most of the authors consider Eq. (4) to represent the hydrogen inhibition effect in the kinetic modelling. This formulation takes into account the effect of both steam and hydrogen on the kinetic of char gasification. However, in this work, the hydrogen inhibition could not be represented using Eq. (4). Therefore, an empiric relation was considered. Indeed, it was found that the ratio of the apparent reaction rate for various hydrogen partial pressures and the one with $P_{\text{H}_2} = 0$ can be well-correlated according to:

$$g(P_{\text{H}_2}) = \frac{R_{\text{app}}(P_{\text{H}_2})}{R_{\text{app}}(P_{\text{H}_2} = 0)} = 1.00 \cdot \left(\frac{P_{\text{H}_2\text{O}}}{P_{\text{H}_2\text{O}} + P_{\text{H}_2}} \right)^{0.74} \quad (16)$$

where $g(P_{\text{H}_2})$ is a function which represents the hydrogen inhibition effect, $R_{\text{app}}(P_{\text{H}_2})$ is the apparent reaction rate for various hydrogen partial pressures and $P_{\text{H}_2\text{O}} = 0.3$ bars, and $R_{\text{app}}(P_{\text{H}_2} = 0)$ is the apparent reaction rate for various steam partial pressures and $P_{\text{H}_2} = 0$ bar.

3.5. Kinetic modelling

3.5.1. Kinetic models

As Reactions (I) and (II) were found to be predominant during the steam gasification of char, a global kinetic model was used to represent experimental results. For the operating conditions considered in this work (i.e. temperature, $P_{\text{H}_2\text{O}}$, P_{H_2}), the Shrinking Core Model (SCM) was found to well-represent the structure function $f(X)$ and was used to estimate the kinetic parameters. This model is presented below.

The SCM (Wen, 1968) assumes that the reaction takes place at the outer surface of a non-porous particle with an initial radius R_0 in isothermal conditions. As the reaction proceeds, the surface moves into the interior of the solid leaving behind an inert ash. By considering a cylindrical particle and a pseudo-steady-state regime, the reaction rate can be expressed as:

$$\frac{dX}{dt} = \frac{2M_c}{R_0 \rho_{t,c} (1 - \varepsilon_p) x_c} A_{\text{SCM}} \cdot \exp\left(-\frac{E_a}{RT_p}\right) \cdot h(P_{\text{H}_2\text{O},s}) \cdot g(P_{\text{H}_2}) \cdot (1 - X)^{1/2} \quad (17)$$

where M_c is the molar weight of carbon (kg mol^{-1}), $\rho_{t,c}$ is the true density of the char (kg m^{-3}), x_c is the mass fraction of carbon in the char particle and A_{SCM} is the pre-exponential

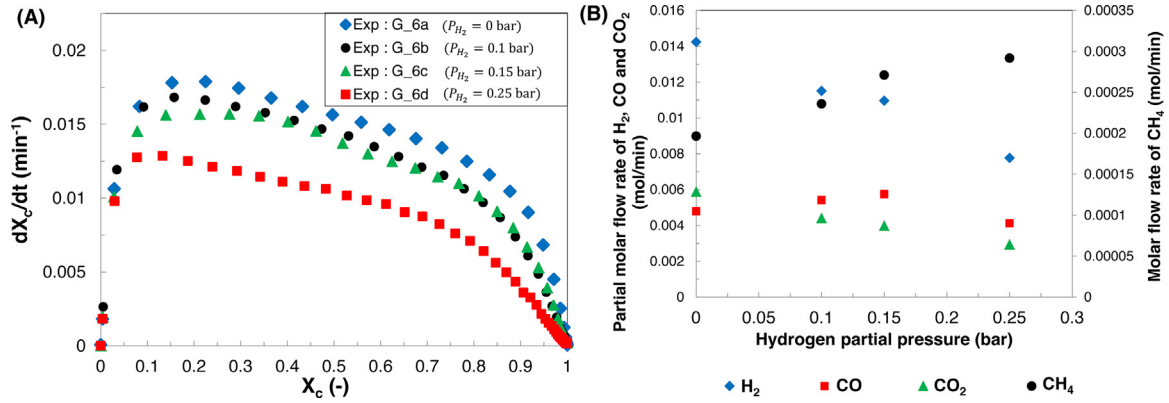


Fig. 14 – Effect of hydrogen partial pressure on (A) the gasification rate versus conversion rate, (B) the molar flow rate of H₂, CO, CO₂ and CH₄ versus hydrogen partial pressure for a given conversion rate of 0.4, (experiments G.6).

factor (mol m⁻² Pa⁻ⁿ s⁻¹), T_p is the particle temperature which is assumed to be equal to that in the bulk.

Besides, the two empirical functions ($h(P_{H_2O,s}) = P_{H_2O,s}^n$ and $g(P_{H_2})$) given in Eq. (16) were considered. To determine the kinetic parameters (i.e. pre-exponential factor, activation energy and reaction order with respect to steam), most of the authors (Irfan et al., 2011) in the literature use a graphical resolution by integrating Eq. (17) and plotting the left hand side versus time:

$$1 - (1 - X)^{1/2} = K_{SCM} \cdot t \quad (18)$$

From the slope of the straight line (Eq. (18)), the kinetic parameters can be determined for various combustion temperatures and steam partial pressures.

3.5.2. Modelling

To obtain the kinetic parameters, a differential equations system was defined which takes into consideration both the effect of gas mixing (i.e. 5 CSTR in series) and the intrinsic kinetic of char gasification (SCM). It is given by the following expression:

$$\text{Kinetic Model} \left\{ \begin{aligned} \frac{dX_{int}}{dt} &= \frac{2M_c}{R_0 \rho_{t,c} (1 - \varepsilon_p) X_c} \cdot \left(\frac{P_{H_2O}}{P_{H_2O} + P_{H_2}} \right)^{0.74} \\ &\cdot A_{SCM} \cdot \exp\left(\frac{E_a}{RT_p}\right) \cdot P_{H_2O}^n \cdot (1 - X_{int})^{1/2} \text{ for the SCM} \end{aligned} \right. \quad (19)$$

$$\text{Effect of gas mixing} \left\{ \begin{aligned} \frac{dX_1}{dt} &= \frac{1}{\tau_{CSTR}} \cdot (X_{int} - X_1) \\ \frac{dX_5}{dt} &= \frac{1}{\tau_{CSTR}} \cdot (X_4 - X_5) \end{aligned} \right.$$

The kinetic parameters A_{SCM} , E_a and n are estimated by solving Eq. (19) using an explicit Runge Kutta (4,5) formula and applying the nonlinear least-squares curve fitting problem which consists in minimizing the sum of the difference between each experimental data and the one corresponding to the model for all temperatures and steam partial pressures according to the following expression:

$$\min_x \|f(x)\|_2^2 = \min_x \left(\sum_{i=1}^N f_i(x)^2 \right) \quad (20)$$

where $f_i(x) = X_{exp} - X_5$, x are the kinetic parameters, N corresponds to the number of experimental data.

In the case of the Shrinking Core Model, the values of pre-exponential factor, activation energy and reaction order with respect to steam are given in Table 6. It can be seen that the

Table 6 – Kinetic parameters obtained with the Shrinking Core Model by solving the differential equations system Eq. (19).

Char type	A_{SCM} (mol m ⁻² Pa ⁻ⁿ s ⁻¹)	E_a (J/mol)	n (-)	$\min_x \ f(x)\ _2^2$
STI650	5.86	122880	0.62	0.2427

activation energy is similar to that obtained in Section 3.4.1. Its value is also in good agreement with those obtained in the literature (see Table 1). The comparisons between experimental data and results obtained from the SCM including the mixing of gas in the sampling lines are given in Figs. 10 and 12. A good agreement is found. The small interval observed may be attributed to the effect of the devolatilization step. Fig. 15(A) also presents the comparison between the SCM and data from experiments G.6. Finally, Fig. 15(B) shows the apparent reaction rate for ($X_c = 0.5$) from the literature and the one proposed in this work. In this figure, the shade area corresponds to 80% of the kinetic model from bibliographic studies. It can be seen that, our kinetic model is in very good agreement compared to those in the literature.

4. Conclusion

This paper presented experimental data on the kinetic of char gasification with steam in a fluidized bed reactor. Experiments were carried out for temperatures in the range of 700–850 °C and steam partial pressures between 0.1 and 0.7 bars. The results showed that the char gasification with steam can be divided into two steps:

- A char devolatilization just after its introduction in the reactor. This step corresponds to a partial degradation of char to form non-condensable products. It depends on the temperature, the char nature and the reactive atmosphere in the reactor. The devolatilization leads to a char conversion less than 5%.
- The second step is the char gasification with steam. It was found that both the reaction between carbon and steam as well as the Water–Gas–Shift reaction are predominant.

The effect of hydrogen partial pressure on the CH₄ production and on the steam gasification was also investigated at atmospheric pressure. First, it was found that interactions between char and hydrogen occur in the reactor. This reaction is very slow and leads to the formation of CH₄. Besides,

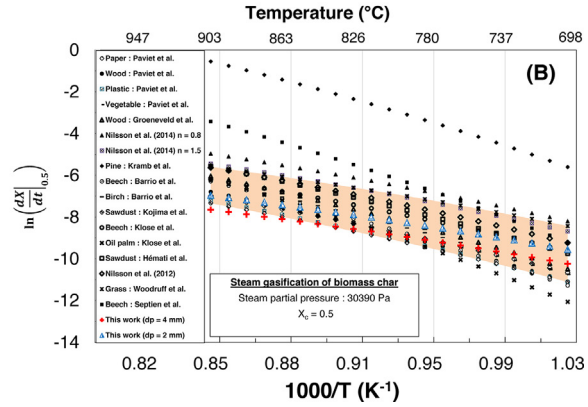
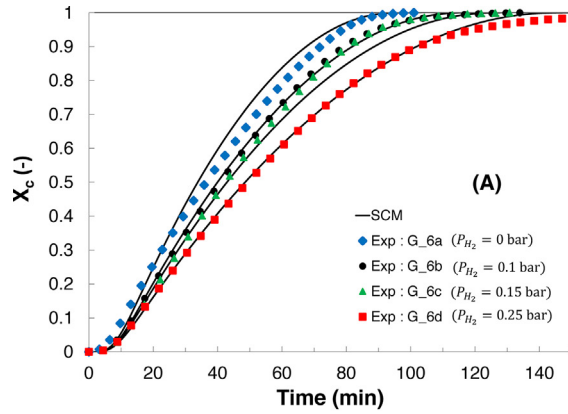


Fig. 15 – (A) Comparison between the SCM obtained from Eq. (19) and experimental data, (B) comparison between apparent reaction rates from literature and the one obtained in this work, Paviet et al. (2007), Groeneveld and van Swaaij (1980), Nilsson et al. (2014, 2012), Kramb et al. (2014), Barrio et al. (2001), Kojima et al. (1993), Klose and Wölki (2005), Hémati and Laguerie (1988), Woodruff and Weimer (2013), Septien et al. (2015).

a higher hydrogen partial pressure leads to a higher methane production. The presence of hydrogen also inhibits the reaction of gasification.

Finally, a global kinetic model was used to represent the experimental steam gasification results. The kinetic modelling includes both the transfer function of the sampling gas lines and the inhibiting effect of hydrogen. The Shrinking Core Model was found to be in good agreement with experimental data. The value of activation energy was equal to 123 kJ/mol while the reaction order with respect to steam was 0.62.

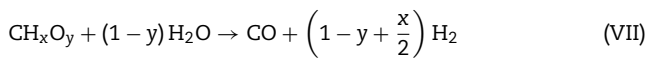
Acknowledgment

The authors thank the “Midi-Pyrénées Region” for financial support of this project.

Appendix A.

Ratio θ

The two following reaction are considered:



The rate of Reactions (VII) and (II) are given by r_1 and r_2 , respectively. The molar flow rates of CO, CO₂ and H₂ are then calculated by the following expressions:

$$\dot{n}_{\text{CO}} = r_1 - r_2 \quad (21)$$

$$\dot{n}_{\text{CO}_2} = r_2 \quad (22)$$

$$\dot{n}_{\text{H}_2} = \left(1-y + \frac{x}{2}\right)r_1 + r_2 \quad (23)$$

By combining Eqs. (21)–(23), we obtain:

$$\dot{n}_{\text{H}_2} = \left(1-y + \frac{x}{2}\right)\dot{n}_{\text{CO}} + \dot{n}_{\text{CO}_2} \left(2-y + \frac{x}{2}\right) \quad (24)$$

Finally, for $x=y=0$, Eq. (24) becomes:

$$\frac{\dot{n}_{\text{H}_2}}{\dot{n}_{\text{CO}} + 2 \cdot \dot{n}_{\text{CO}_2}} = 1 \quad (25)$$

References

- Ahmed, I.I., Gupta, A.K., 2011. Kinetic of woodchips char gasification with steam and carbon dioxide. *Appl. Energy* 88, 1613–1619.
- Barrio, M., Gøbel, B., Risnes, H., Henriksen, U., Hustad, J.E., Sørensen, L.H., 2001. Steam gasification of wood char and the effect of hydrogen inhibition on the chemical kinetics. *Conference on Progress in Thermochemical Biomass Conversion*.
- Bates, R.B., Altantzis, C., Ghoniem, A.F., 2016. Modeling of biomass char gasification, combustion, and attrition kinetics in fluidized beds. *Energy Fuels* 30, 360–376.
- Bathia, S.K., Perlmutter, D.D., 1980. A random pore model for fluid-solid reaction: I. Isothermal kinetic control. *AIChE J.* 26, 379–386.
- Bhat, A., Bheemarasetti, J.V.R., Rao, T.R., 2001. Kinetic of rice husk char gasification. *Energy Convers. Manage.* 42, 2061–2069.
- Blackwood, J.D., McGrory, F., 1958. The carbon-steam reaction at high pressure. *Aust. J. Chem.* 11, 16–23.
- Chen, C., Zhang, S., Xu, K., Luo, G., Yao, H., 2015. Experimental and modeling study of char gasification with mixtures of CO₂ and H₂O. *Energy Fuels* 30, 1628–1635.
- Di Blasi, C., 2008. Modeling chemical and physical processes of wood and biomass pyrolysis. *Prog. Energy Combust. Sci.* 34, 47–90.
- Di Blasi, C., 2009. Combustion and gasification rates of lignocellulosic chars. *Prog. Energy Combust. Sci.* 35, 121–140.
- Dupont, C., Jacob, S., Marrakchy, K.O., Hognon, C., Grateau, M., Labalette, F., Da Silva Perez, D.V., 2016. How inorganic elements of biomass influence char steam gasification kinetics. *Energy* 109, 430–435.
- Dutta, S., Wen, C.Y., 1977. Reactivity of coal and char. 2. In oxygen-nitrogen atmosphere. *Ind. Eng. Chem. Process Des. Dev.* 16, 31–37.
- Gómez-Barea, A., Leckner, B., 2010. Modeling of biomass gasification in fluidized bed. *Prog. Energy Combust. Sci.* 36, 444–509.
- González, J.F., Ramiro, A., Sabio, E., Encinar, J.M., González, C.M., 2002. Hydrogasification of almond shell chars. Influence of operating variables and kinetic study. *Ind. Eng. Chem. Res.* 41, 3557–3565.
- Groeneveld, M.J., van Swaaij, W.P.M., 1980. Gasification of char particles with CO₂ and H₂O. *Chem. Eng. Sci.* 35, 307–313.

- Hémami, M., Laguerie, C., 1988. Determination of the kinetic of the wood sawdust steam gasification of charcoal in a thermobalance. *Entropie* 142, 29–40.
- Hüttinger, K.J., Merdes, W.F., 1992. The carbon-steam reaction at elevated pressure: formations of product gases and hydrogen inhibitions. *Carbon* 30, 883–894.
- Hüttinger, K., 1988. Mechanism of water vapor gasification at high hydrogen levels. *Carbon* 26, 79–87.
- Hawley, M.C., Boyd, M., Anderson, C., DeVera, A., 1983. Gasification of wood char and effects of intraparticle transport. *Fuel* 62, 213–216.
- Hofbauer, H., Rauch, R., Löffler, G., Kaiser, S., 2002. Six years experience with the FICFB-gasification process. In: Presented at the 12th European Conference and Technology Exhibition on Biomass for Energy, Industry and Climate Protection, Amsterdam, The Netherlands.
- Irfan, M.F., Usman, M.R., Kusakabe, K., 2011. Coal gasification in CO₂ atmosphere and its kinetics since 1948: a brief review. *Energy* 36, 12–40.
- Khawam, A., Flanagan, D.R., 2010. Solid-state kinetic models: basics and mathematical fundamentals. *J. Phys. Chem. B* 110, 17315–17328.
- Klinghoffer, N.B., Castaldi, M.J., Nzihou, A., 2012. Catalyst properties and catalytic performance of char from biomass gasification. *Ind. Eng. Chem. Res.* 51, 13113–13122.
- Klose, W., Wölki, M., 2005. On the intrinsic reaction rate of biomass char gasification with carbon dioxide and steam. *Fuel* 84, 885–892.
- Kojima, T., Assavadakorn, P., Furusawa, T., 1993. Measurement and evaluation of gasification kinetics of sawdust char with steam in an experimental fluidized bed. *Fuel Process. Technol.* 36, 201–207.
- Kramb, J., Kontinen, J., Gómez-Barea, A., Moilanen, A., Umeki, K., 2014. Modeling biomass char gasification kinetics for improving prediction of carbon conversion in a fluidized bed gasifier. *Fuel* 132, 107–115.
- Laurendeau, N.M., 1978. Heterogeneous kinetics of coal char gasification and combustion. *Prog. Energy Combust. Sci.* 4, 221–270.
- Le, C.D., Kolaczkowski, S.T., 2015. Steam gasification of a refuse derived char: reactivity and kinetics. *Chem. Eng. Res. Des.* 102, 389–398.
- Liu, X., Xiong, B., Huang, X., Ding, H., Zheng, Y., Liu, Z., Zheng, C., 2017. Effect of catalysts on char structural evolution during hydrogasification under high pressure. *Fuel* 188, 474–482.
- Lussier, M.G., Zhang, Z., Miller, D.J., 1998. Characterizing rate inhibition in steam/hydrogen gasification via analysis of adsorbed hydrogen. *Carbon* 36, 1361–1369.
- Marquez-Montesinos, F., Cordero, T., Rodríguez-Mirasol, J., Rodríguez, J.J., 2002. CO₂ and steam gasification of a grapefruit skin char. *Fuel* 81, 423–429.
- Mermoud, F., Salvador, S., Van de Steene, L., Golfier, F., 2006. Influence of the pyrolysis heating rate on the steam gasification rate of large wood char particles. *Fuel* 85, 1473–1482.
- Morin, M., Pécate, S., Hémami, M., Kara, Y., 2016. Pyrolysis of biomass in a batch fluidized bed reactor: effect of the pyrolysis conditions and the nature of the biomass on the physicochemical properties and reactivity of char. *J. Anal. Appl. Pyrolysis* 122, 511–523.
- Morin, M., Pécate, S., Hémami, M., 2018. Kinetic study of biomass char combustion in a low temperature fluidized bed reactor. *Chem. Eng. J.* 331, 265–277.
- Morin, M., Pécate, S., Masi, E., Hémami, M., 2017. Kinetic study and modelling of char combustion in TGA in isothermal conditions. *Fuel* 203, 522–536.
- Nandi, S.P., Onischak, M., 1985. Gasification of chars obtained from maple and jack pine woods. *Fundam. Thermochem. Biomass Convers.*, 567–587.
- Nilsson, S., Gómez-Barea, A., Fuentes Cano, D., 2012. Gasification reactivity of char from dried sewage sludge in a fluidized bed. *Fuel* 92, 346–353.
- Nilsson, S., Gómez-Barea, A., Fuentes-Cano, D., Campoy, M., 2014. Gasification kinetics of char from olive tree pruning in fluidized bed. *Fuel* 125, 192–199.
- Paviet, F., Bals, O., Antonini, G., 2007. Kinetic study of various chars steam gasification. *Int. J. Chem. React. Eng.* 5, 1–14.
- Roberts, D.G., Harris, D.J., 2006. A kinetic analysis of coal char gasification reactions at high pressures. *Energy Fuels* 20, 2314–2320.
- Roberts, D.G., Harris, D.J., 2007. Char gasification in mixtures of CO₂ and H₂O: competition and inhibition. *Fuel* 86, 2672–2678.
- Ruiz, J.A., Juárez, M.C., Morales, M.P., Muñoz, P., Mendivil, M.A., 2013. Biomass gasification for electricity generation: review current technology barriers. *Renew. Sustain. Energy Rev.* 18, 174–183.
- Septien, S., Escudero Sanz, F.J., Salvador, S., Valin, S., 2015. Steam gasification of char from wood chips fast pyrolysis: development of a semi-empirical model for a fluidized bed reactor application. *Biomass Bioenergy* 77, 64–74.
- Szekely, J., Evans, J.W., Sohn, H.Y., 1976. *Gas-solid Reactions*. Academic Press, New York.
- Vyazovkin, S., Burnham, A.K., Criado, J.M., Pérez-Maquada, L.A., Popescu, C., Sbirrazzuoli, N., 2011. ICTAC kinetic committee recommendations for performing kinetic computations on thermal analysis data. *Thermochim. Acta* 520, 1–19.
- Wen, C.Y., 1968. Noncatalytic heterogeneous solid fluid reaction models. *Ind. Eng. Chem.* 60, 34–54.
- Woodruff, R.B., Weimer, A.W., 2013. A novel technique for measuring the kinetics of high-temperature gasification of biomass char with steam. *Fuel* 103, 749–757.
- Zhai, M., Zhang, Y., Dong, P., Liu, P., 2015. Characteristic of rice husk char gasification with steam. *Fuel* 158, 42–49.